A CRITICAL ASSESSMENT OF CRACK GROWTH CRITERIA IN UNIDIRECTIONAL COMPOSITES

by

Andre Barbe

Thesis submitted to the Faculty of the Virginia Polytechnic Institute and State University in partial fulfillment of the requirements for the degree of

Master of Science

in

Engineering Mechanics

APPROVED:

C. T. Herakovich, Chairman

C. W. Smith

M. J. Pindera

August 1985

Blacksburg, Virginia

A CRITICAL ASSESSMENT OF CRACK GROWTH CRITERIA IN UNIDIRECTIONAL COMPOSITES

by

Andre Barbe

(ABSTRACT)

The problem examined is an infinite anisotropic layer with a through crack at arbitrary orientation, subjected to uniform in-plane remote loading. The purpose of this study is to gain a better understanding of several theoretical models for predicting the direction of crack propagation and the level of load causing crack extension, and to present a new model for predicting the critical load. The discussed models are particularly examined in detail with regard to the physical parameters affecting the results. Comparison is made with available experimental results. It is shown that the normal stress ratio theory provides good agreement with experimental crack growth direction, independant of physical parameters, and that the newly proposed traction ratio theory predicts well the critical load causing crack extension.

Acknowledgements

The author wishes to express his sincere thanks to Dr. Herakovich for his very friendly and patient guidance during this research, and Dr. Smith and Dr. Pindera for their help and contribution to the author's knowledge in composite materials.

The author is also grateful to the company C.d.F. Chimie and the French government for their financial assistance which made possible this very interesting year of study.

A special thanks goes to Mrs. Neta Byerly for the very good work she did in typing this thesis.

Table of Contents

Table of Contents (continued)

Page

Table of Contents (continued)

List of Figures

List of Figures (continued)

List of Tables

1.0 Introduction

1.0 Introduction

1.1 Motivation of the Study

The propagation of a crack in unidirectional filamentary composite material can occur in two very different ways, either breaking the fibers or propagating between fibers. It can be difficult to determine whether fiber failure will occur. However, knowledge of the direction of propagation is crucial for determining the level of load causing crack extension. Several criteria predicting the direction of crack propagation and the load causing extension have been proposed previously. They are based on different physical approaches and hypotheses. A study of the influence of the parameters involved in each theory and a comparison with experimental results can provide necessary verification for the choice of a reliable criteria for crack growth.

1.2 Literature Review

The problem of crack growth in composite materials has been analyzed in several different ways by many researchers. Most of the crack propagation theories include the hypothesis of the homogeneity of the material. Among these are the theories which are extensions of classical fracture mechanics developed for isotropic materials. The strain energy density theory, elaborated by G. Sih ([1] and [2]) has been extended without modification to composite materials and has been applied successfully to the prediction of the applied critical load in several cases [3]. The tensor polynomial theory [4], proposed for the failure of unnotched lamina, has been applied to laminates [5]. The normal stress ratio theory, specially developed for notched composites, has been applied successfully to the determination of the direction of crack propagation [6]. The point stress criteria of Whitney and Nuismer [7], based on the determination of the stresses at a finite distance from the crack tip, can explain size effects that the classical theory of stress intensity factors does not take into account.

Some theories have attempted to take into account the inhomogeneity of the material. However, most of them have been applied only to special cases of crack orientation and loading direction with respect to the fiber orientation. Among those is the matrix model of the strain energy density theory [8]. It has been applied successfully to cracks parallel to the fibers; this application requires the solution of a three phase model. The general fracture toughness parameter theory of C. C. Poe and J. A. Sova [9] is based upon the determination of the strain in the fibers near the crack tip. It has been applied to cracks perpendicular to the fibers. The Hedgepeth model [10] entails the determination of a stress concentration factor at the vicinity of broken fibers. It uses a shear-lag method.

As it appears above, each theory is based on a different physical concept (energy, stress tensor, stress component, strain...). They has been applied successfully to one or several particular classes of problem. However, no single theory has yet been proven to be reliable in the majority of the cases experimentally encountered. Moreover, few comparisons between two or more of the theories have been carried out, either from the theoretical point of view or in a comparison with experimental results. These comparisons would be particularly useful for the fundamental problem of a crack imbedded in a single layer of an unidirectional composite material, as the investigation of this basic problem could bring decisive arguments regarding the use of a particular criteria to solve the more complex problems that are encountered in composite structures.

2.0 Problem Statement

2.1 Hypotheses and Notations

The subject of the present study is a straight crack embedded in an infinite layer of a fibrous composite material (Fig. 2.1). This layer is subjected to a uniform far field loading, characterized by $\bar{\sigma}_x$, $\bar{\sigma}_y$, $\bar{\tau}_{xy}$. The following hypotheses have been assumed:

- The material is linear, elastic, homogeneous and anisotropic.
- The state of stress is two-dimensional.

2.2 Elastic Solutions

The application of the crack growth criteria studied in the next chapter requires the knowledge of the state of stress in the plane. The determination of the stresses σ_x, σ_y τ_{xy} can be reduced to the determination of two potential functions ϕ_1 and ϕ_2 such that [11]:

$$\sigma_x = 2\mathrm{Re}[S_1^2\phi_1^{'}\ (Z_2) + S_2^2\phi_2^{'}\ (Z_2)]$$

$$\sigma_y = 2\mathrm{Re}[\phi_1^{'}\ (Z_1) + \phi_2^{'}(Z_2)]$$

$$\tau_{xy} = -2\mathrm{Re}[S_1\phi_1^{'}\ (Z_1) + S_2\phi_2^{'}\ (Z_2)] \qquad (2.1)$$

with: $Z_1 = x + S_1y$ and $Z_2 = x + S_2y$

S_1 and S_2 are two non-conjugate solutions to the following characteristic equation, involving the extensional stiffness matrix

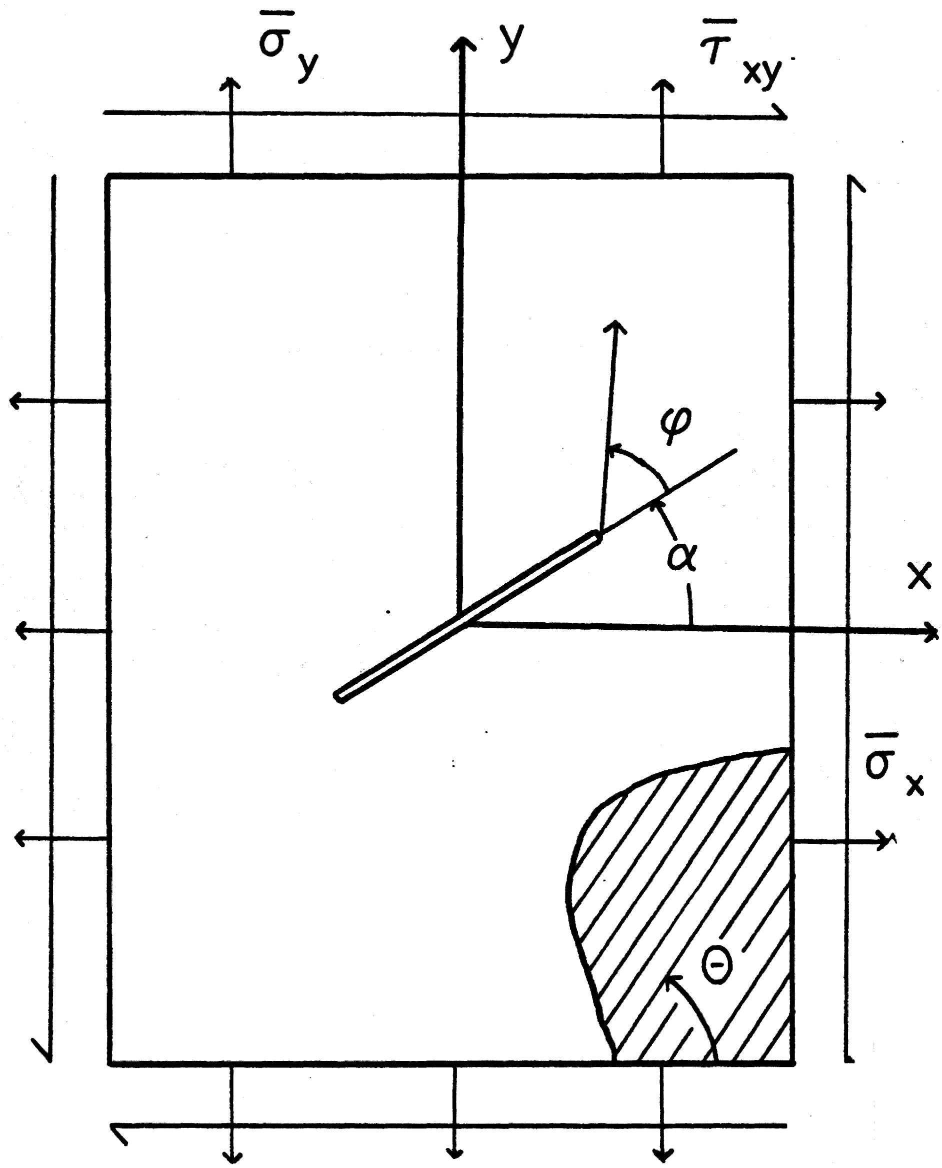

Fig. 2.1 Infinite Center Cracked Plate Under Biaxial Tension

coefficients of the plate A_{ij}:

$$A_{11}S^4 + A_{16}S^3 + (2A_{12} + A_{66})S^2 - 2A_{26}S + A_{22} = 0 \qquad (2.2)$$

Two different elastic solutions for the problem depicted in Fig. 2.1 are currently available in the literature. One is an approximate solution, giving the singular stress field at the neighborhood of the crack tip. The other one is the exact solution, including singular and non singular terms.

In order to simplify the notation, the stresses will be given for a crack angle α equal to zero in the following two sections. The case $\alpha \neq 0^0$ can be obtained by an appropriate rotation of the stress tensor. The half crack length and the distance from the crack tip will be called a and r, respectively.

2.2.1 Approximate Elastic Solution

This solution satisfies the boundary conditions at the crack surface only. From Savin [12], the complex potential functions of eq 2.1 are:

$$\phi_1 (Z_1) = - \frac{a(S_2 \bar{\sigma}_y + \bar{\tau}_{xy})}{2(S_1 - S_2)} \left(\frac{\zeta_1}{a}\right)^{1/2}$$

$$\phi_2 (Z_2) = \frac{a(S_1\bar{\sigma}_y + \bar{\tau}_{xy})}{2(S_1 - S_2)} \left(\frac{\zeta_2}{a}\right)^{1/2} \qquad (2.3)$$

where

$$\zeta_1 = r(\cos\phi + S_1\sin\phi) = Z_1 - a$$

$$\zeta_2 = r(\cos\phi + S_2\sin\phi) = Z_2 - a$$

These potential functions yield the stress distribution near the crack tip:

$$\sigma_x = \frac{\bar{\sigma}_y\sqrt{a}}{\sqrt{2r}}\,\mathrm{Re}\left\{\frac{S_1S_2}{(S_1 - S_2)}\left[\frac{S_2}{\psi_2^{1/2}} - \frac{S_1}{\psi_1^{1/2}}\right]\right\} + \frac{\bar{\tau}_{xy}\sqrt{a}}{\sqrt{2r}}\,\mathrm{Re}\left\{\frac{1}{(S_1 - S_2)}\left[\frac{S_2^2}{\psi_2^{1/2}} - \frac{S_1^2}{\psi_1^{1/2}}\right]\right\}$$

$$\sigma_y = \frac{\bar{\sigma}_y\sqrt{a}}{\sqrt{2r}}\,\mathrm{Re}\left\{\frac{1}{(S_1 - S_2)}\left[\frac{S_1}{\psi_2^{1/2}} - \frac{S_2}{\psi_1^{1/2}}\right]\right\} + \frac{\bar{\tau}_{xy}\sqrt{a}}{\sqrt{2r}}\,\mathrm{Re}\left\{\frac{1}{(S_1 - S_2)}\left[\frac{1}{\psi_2^{1/2}} - \frac{1}{\psi_1^{1/2}}\right]\right\} \qquad (2.4)$$

$$\tau_{xy} = \frac{\bar{\sigma}_y\sqrt{a}}{\sqrt{2r}}\,\mathrm{Re}\left\{\frac{S_1S_2}{(S_1 - S_2)}\left[\frac{1}{\psi_1^{1/2}} - \frac{1}{\psi_2^{1/2}}\right]\right\} + \frac{\bar{\tau}_{xy}\sqrt{a}}{\sqrt{2r}}\,\mathrm{Re}\left\{\frac{1}{(S_1 - S_2)}\left[\frac{S_1}{\psi_1^{1/2}} - \frac{S_2}{\psi_2^{1/2}}\right]\right\}$$

where $\psi_1 = \cos\phi + S_1\sin\phi = \frac{\zeta_1}{r}$ and $\psi_2 = \cos\phi + S_2\sin\phi = \frac{\zeta_2}{r}$

2.2.2. COMPLETE ELASTICITY SOLUTION

This solution (see for example Wu [13]), satisfies the stressfree boundary conditions on the crack surface as well as the far field applied stress condition. The potentials ϕ_1 and ϕ_2 are:

$$\phi_1 = \frac{a^2(S_2\,\bar{\sigma}_y + \bar{\tau}_{xy})}{2(S_1 - S_2)\,(Z_1 + \sqrt{Z_1^2 - a^2})}$$

$$\phi_2 = -\frac{a^2(S_1\,\bar{\sigma}_y + \bar{\tau}_{xy})}{2(S_1 - S_2)(Z_2 + \sqrt{Z_2^2 - a^2})} \tag{2.5}$$

The stresses are given by:

$$\sigma_x = \bar{\sigma}_x + \mathrm{Re}\,\Big[S_1^2\,\Big(\frac{S_2\,\bar{\sigma}_y + \bar{\tau}_{xy}}{S_1 - S_2}\Big)\Big(\frac{(Z_1^2 - a^2)^{1/2} - Z_1}{(Z_1^2 - a^2)^{1/2}}\Big)$$

$$- S_2^2\,\Big(\frac{S_1\bar{\sigma}_y + \bar{\tau}_{xy}}{S_1 - S_2}\Big)\Big(\frac{(Z_2^2 - a^2)^{1/2} - Z_2}{(Z_2^2 - a^2)^{1/2}}\Big)\Big]$$

$$\sigma_y = \bar{\sigma}_y + \mathrm{Re}\,\Big[\Big(\frac{S_2\,\bar{\sigma}_y + \bar{\tau}_{xy}}{S_1 - S_2}\Big)\Big(\frac{(Z_1^2 - a^2)^{1/2} - Z_1}{(Z_1^2 - a^2)^{1/2}}\Big)$$

$$- \Big(\frac{S_2\,\bar{\sigma}_y + \bar{\tau}_{xy}}{S_1 - S_2}\Big)\Big(\frac{(Z_2^2 - a^2)^{1/2} - Z_2}{(Z_2^2 - a^2)^{1/2}}\Big)\Big]$$

$$\tau_{xy} = \bar{\tau}_{xy} - \mathrm{Re}\,\Big[S_1 \left(\frac{S_2\,\bar{\sigma}_y + \bar{\tau}_{xy}}{S_1 - S_2} \right) \left(\frac{(Z_1^2 - a^2)^{1/2} - Z_1}{(Z_1^2 - a^2)^{1/2}} \right)$$

$$- S_2 \left(\frac{S_1\,\bar{\sigma}_y + \bar{\tau}_{xy}}{S_1 - S_2} \right) \left(\frac{(Z_2^2 - a^2)^{1/2} - Z_2}{(Z_2^2 - a^2)^{1/2}} \right) \Big] \qquad (2.6)$$

These stresses have the disadvantage of being non-linear in $r^{-1/2}$, contrary to the singular stress functions discussed previously. At a short distance from the crack tip, the difference between the two solutions for (eq 2.4 and 2.6) is negligible. A plot showing an example of the difference between these solutions for σ_4 is shown in Fig. 2.2. For T300/5208 Gr/Ep and the geometry corresponding to Fig. 2.2 ($\theta = 45°$), this difference is always less than 25% when r/a is less than 0.5.

The difference between the two solutions approaches zero when r/a approaches zero, and goes to the far-field loading when r/a goes to infinity. This is illustrated by Fig. 2.3, which shows $\Delta\sigma_y$ versus Log (r/a) on the crack line, for the same geometry and material as in Fig. 2.2. $\Delta\sigma_y$ is defined to be σ_y predicted by the complete solution minus σ_y predicted by the approximate solution.

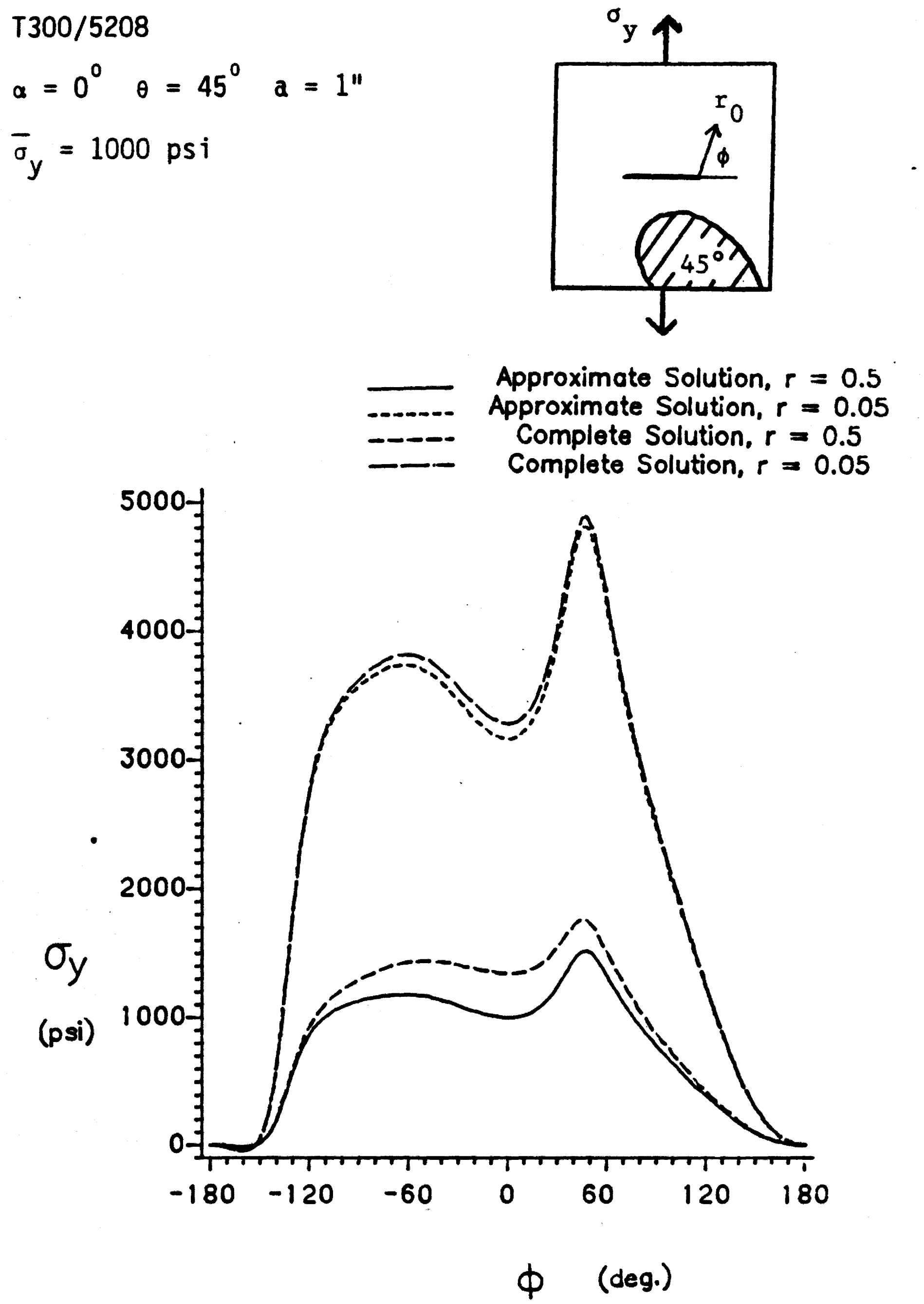

Fig. 2.2 σ_y Versus ϕ for the Approximate and the Complete Elastic Solutions

T300/5208

$\alpha = 0^0 \quad \theta = 45^0$

$\bar{\sigma}_y = 1000$ psi

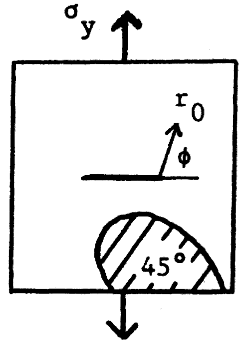

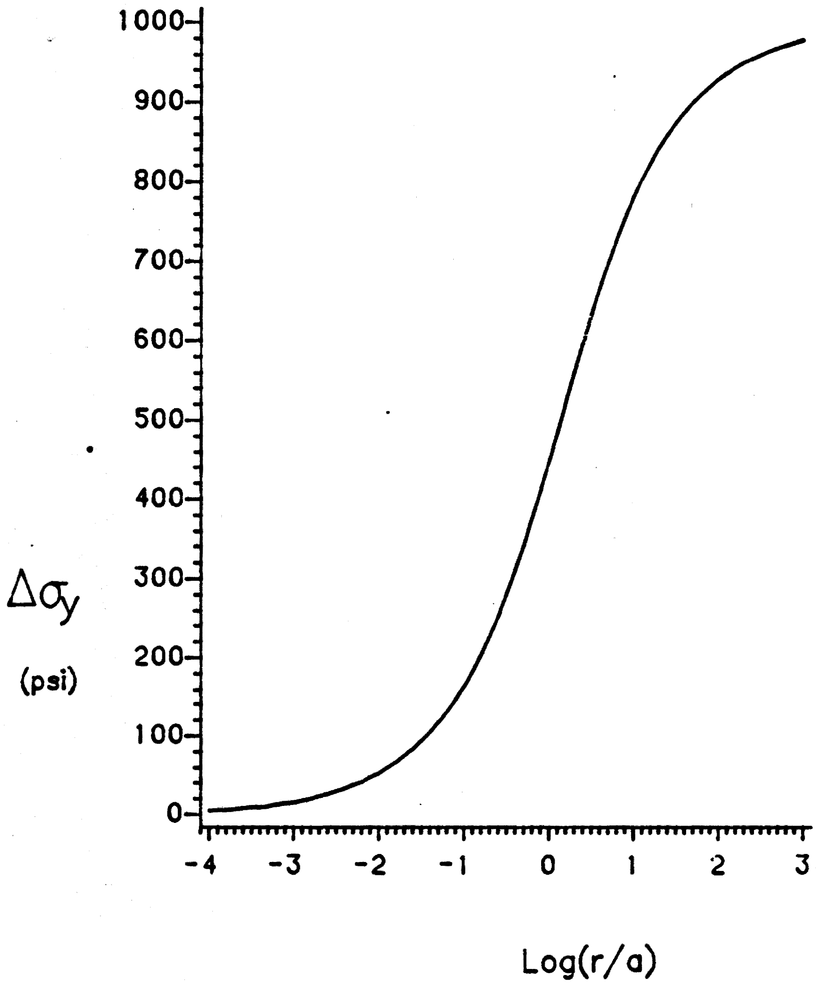

Fig. 2.3 $\Delta\sigma_y$ Versus Log (r/a)

3.0 Criteria for Crack Growth

3.1 Tensor Polynomial Theory

3.1.1 The Tensor Polynomial Theory for Crack Growth

This criterion is based on the existence of a convex failure surface represented by a polynomial equation. Typically, a second order polynomial is assumed. Using contracted notation:

$$P(\{\sigma\}) = F_i\sigma_i + F_{ij}\sigma_i\sigma_j \tag{3.1}$$

$\{\sigma\}$ being the stress tensor and σ_i its components in contracted notation.

Wu [5] defines two vectorial quantities in stress space, the stress vector and the strength vector. The stress vector is:

$$\vec{s} = \sigma_i\vec{e}_i \tag{3.2}$$

(e_i, i = 1, 6) being the unit vectors of the stress space. The strength vector is:

$$\vec{f} = \sigma_i^*\vec{e}_i \tag{3.3}$$

$\{\sigma^*\}$ being a stress tensor proportional to $\{\sigma\}$, such that $P(\{\sigma^*\}) = 1$.

These two vectors are computed at a specified distance r_o from the crack tip, r_o being a characteristic of the material. The amplitudes of the two vectors can be represented as a function of the angle ϕ (Fig. 3.1).

Failure occurs when the contour of the stress vector first becomes tangent to the contour of the strength vector as the loading is increased. The angle where these two curves meet is the predicted direction of crack propagation ϕ_c.

3.1.2 Role of the Parameters

According to Wu [5], the distance r_o is an important characteristic of the material. Its value is found experimentally by testing various cases of mixed loading modes to failure. For Gℓ/Ep, Wu found r_o = 0.076" for fracture under far-field tension and r_o = 0.077" for fracture under far-field shear [5]. When the half crack length a is comparable to r_o, the non-singular stresses are of the same order of magnitude as the singular stresses, therefore a complete elastic solution must be used for small a (see chapter 2.2 and Fig. 2.2).

The predictions for the angle corresponding to the largest value of the tensor polynomial are sometime very sensitive to the value of r_o. As an illustration, two plots of the tensor polynomial versus the angle ϕ are given in Fig. 3.2 for a specimen studied in detail in Chapter 4. For r_o = 0.0029", the maximum value of the tensor polynomial occurs at $\phi = 82^0$ (which is close to the experimentally

T300/5208

$\alpha = 45^0 \quad \theta = 90^0 \quad a = 1" \quad r_0 = 0.08"$

$\bar{\sigma}_y = 2970$ psi

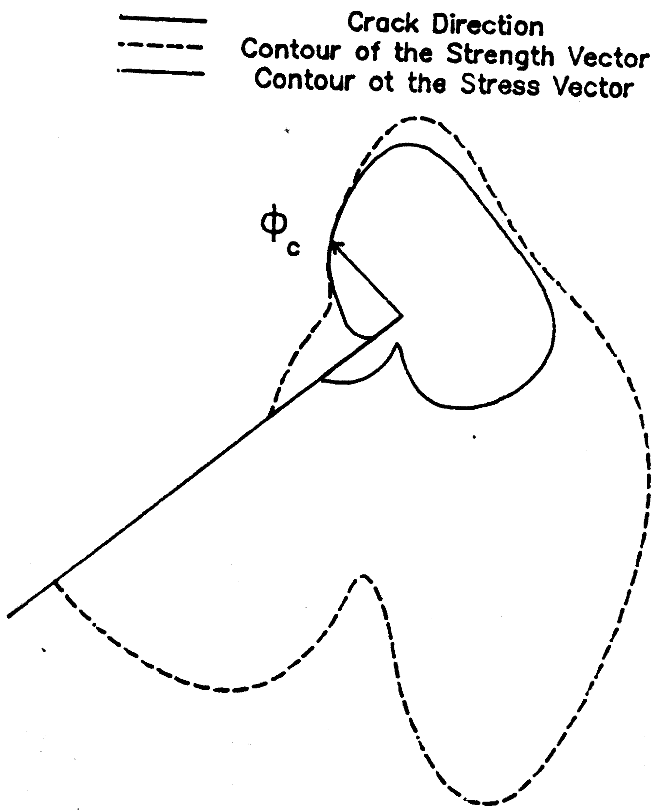

Fig. 3.1 Contour of the Stress and Strength Vectors

AS4/3501-6

$\alpha = -15^{0}$ $\theta = 75^{0}$ $a = 0.1"$

$r_0 = 0.002"$: $\bar{\sigma}_y = 8071$ psi $\bar{\tau}_{xy} = 1792$ psi

$r_0 = 0.0029"$: $\bar{\sigma}_y = 9139$ psi $\bar{\tau}_{xy} = 2029$ psi

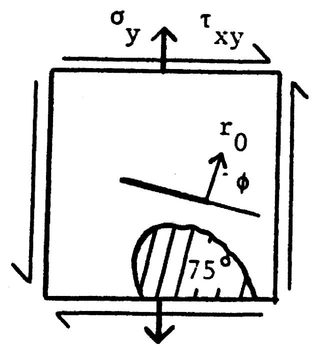

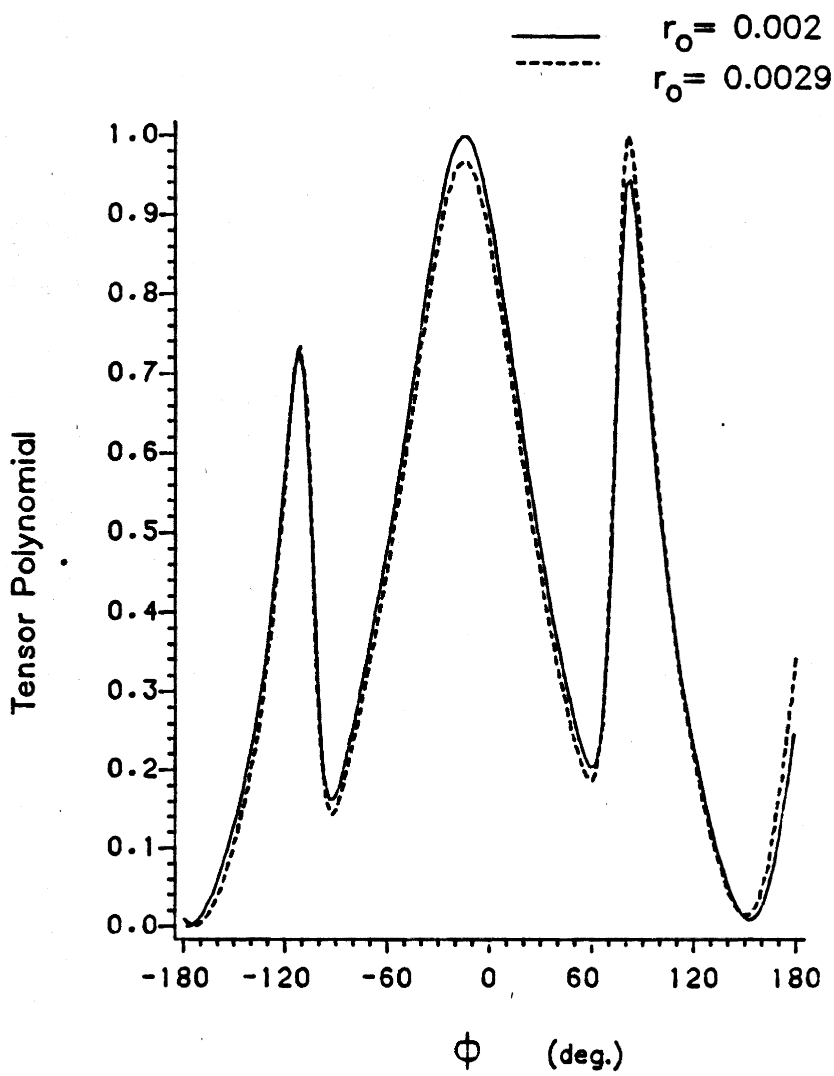

Fig. 3.2 Tensor Polynomial Versus ϕ at Two Different r_0

observed angle of propagation, 75°); at r_0 = 0.002", the maximum value is at $\phi = -15^0$.

3.1.3 Typical Results for Crack Growth Direction Prediction

Two curves giving the angle of crack extension ϕ_c as a function of the fiber orientation θ for simple tension and simple shear are given in Fig. 3.3. The material properties are those of T300/5208 Gr/Ep, given in Appendix C. The value of r_0, 0.08 inches, is the same used by Wu [13]. The half crack length a has been chosen equal to 1. The ratio r_0/a is small, therefore the non-singular terms in the complete elastic solution do not play an important role here. For simple tensile loading, two important results become apparent:

- for $\theta = 90^0$ (crack perpendicular to the fibers), a self-similar propagation is predicted by the theory.
- for $\theta = 0^0$ (crack parallel to the fiber), the propagation initiates at an angle of 46° from the original crack direction.

Both results are contrary to experimental observation for Gr/Ep. It is possible that the choice of the interaction term F_{12} could influence this prediction significantly. This term is difficult to measure and a broad range of values has been reported in the literature. The influence of F_{12} on the prediction of the crack extension direction can be determined by theoretical considerations. As the failure surface in the stress space must be closed, the values

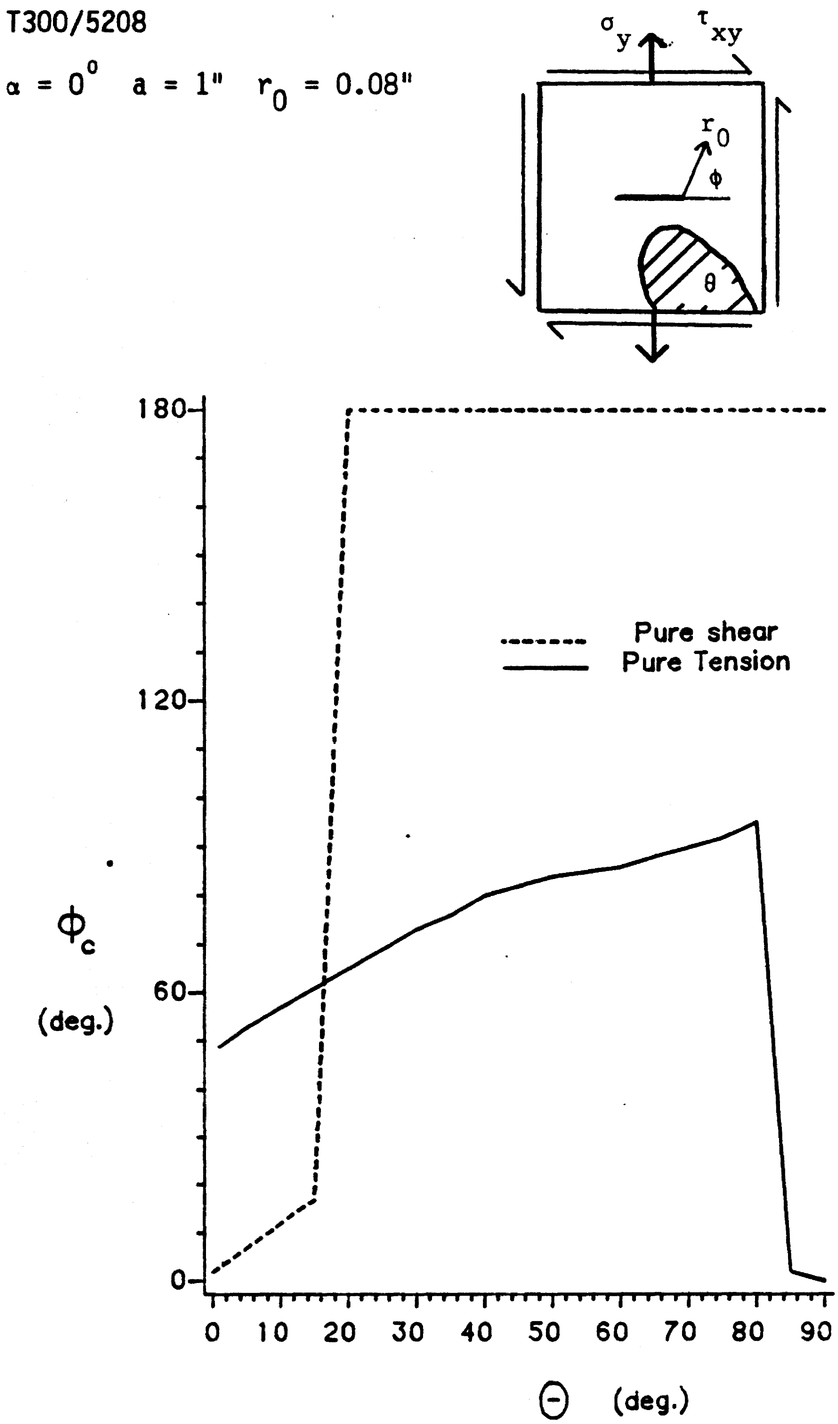

Fig. 3.3 Critical Angle (ϕ_c) Predicted by the Tensor Polnomial Theory Versus the Fibre Orientation (θ)

taken by this interaction term must be between $-\sqrt{F_{11}F_{22}}$ and $\sqrt{F_{11}F_{22}}$. For $\theta = 0$, a variation of F_{12} in the full admissible range predicts a variation of ϕ_c of only a few degrees (4.25 for T300/5208). As an illustration, Figs. 3.4 and 3.5 are two curves showing ϕ_c and σ_y at failure versus a parameter K, varying from -1 to +1, and defined as:

$$K = \frac{F_{12}}{\sqrt{F_{11}F_{22}}} \tag{3.4}$$

The dependence of load at failure on F_{12} is also surprisingly low.

A surprising result is the dependance of ϕ_c on the half crack length a (Fig. 3.6). This is primarily due to the choice of the complete elastic solution for the stresses. It induces a coupling between the variables a and ϕ in the tensor polynomial. Even with the approximate solution, since the ultimate tensile and compressive strengths are different, this coupling would occur due to the presence of linear and quadratic terms in the tensor polynomial (see eq. 3.1).

Figure 3.6 shows a variation of 30 degrees for the angle ϕ_c (solid line). If the approximate elastic solution is used, the variation is only one degree (dotted line).

3.2.0 Strain Energy Density Theory

3.2.1 Presentation of the Theory

Sih [1] defines the strain energy density factor as

$$S = W \times r \tag{3.5}$$

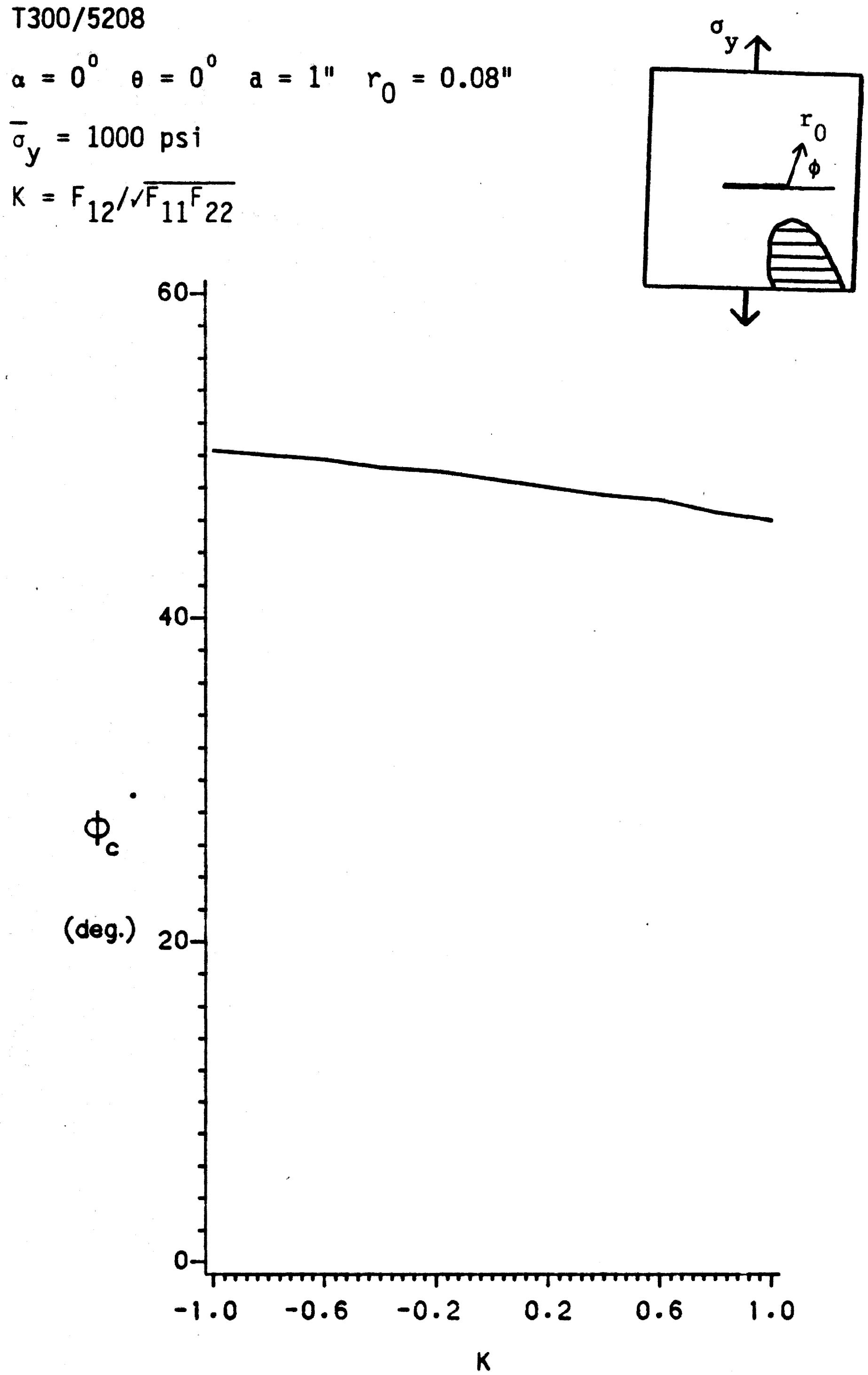

Fig. 3.4 Critical Angle (ϕ_c) Predicted by the Tensor Polynomial Theory Versus K

T300/5208

$\alpha = 0^\circ$ $\theta = 0^\circ$ $a = 1"$ $r_0 = 0.08"$

$\bar{\sigma}_y = 1000$ psi

$K = F_{12}/\sqrt{F_{11}F_{22}}$

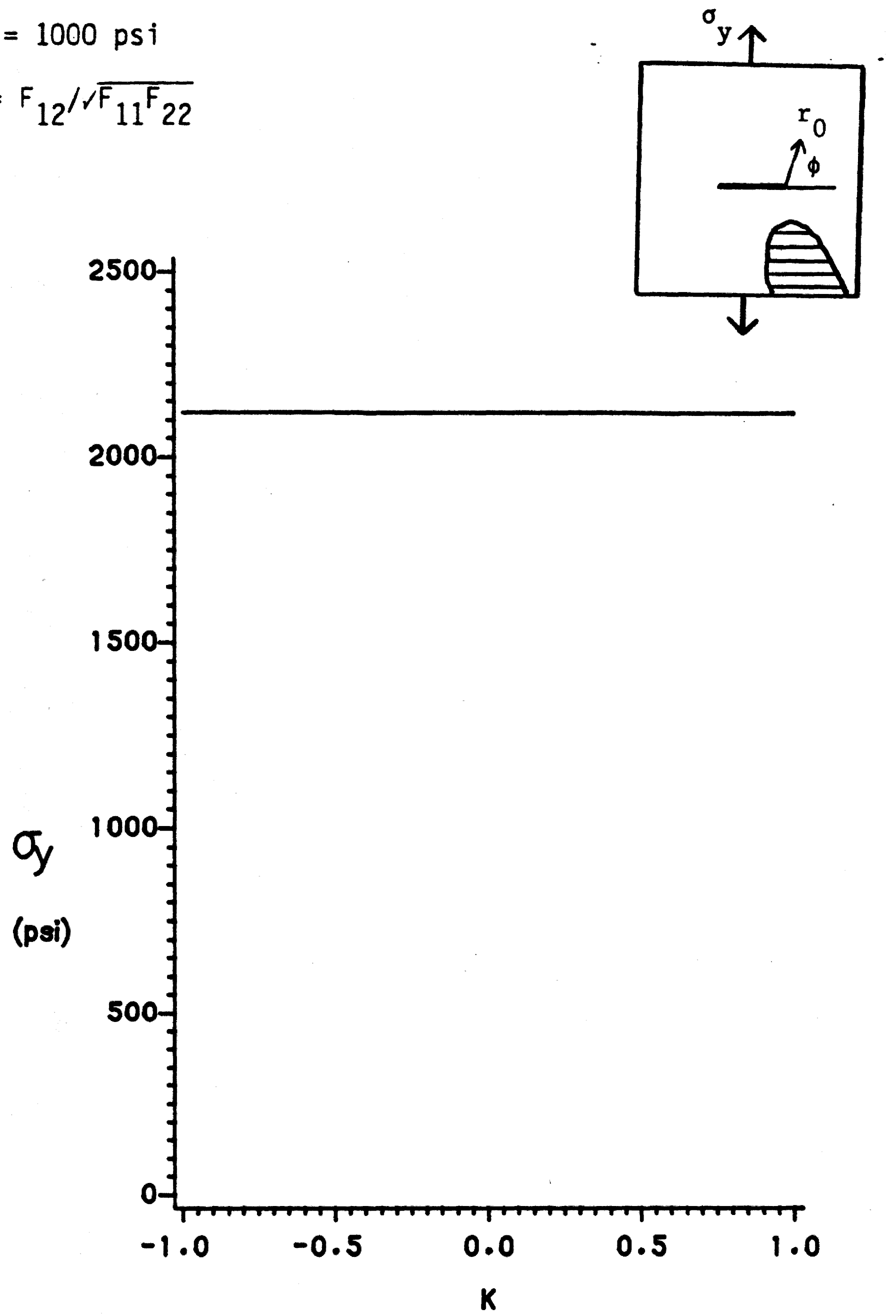

Fig. 3.5 Load at Failure (σ_y) Predicted by the Tensor Polynomial Theory Versus K.

T300/5208

$\alpha = 0^o$ $\theta = 0^o$ $a = 1"$ $r_0 = 0.08"$

$\bar{\sigma}_y = 1000$ psi

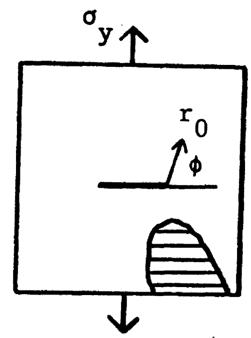

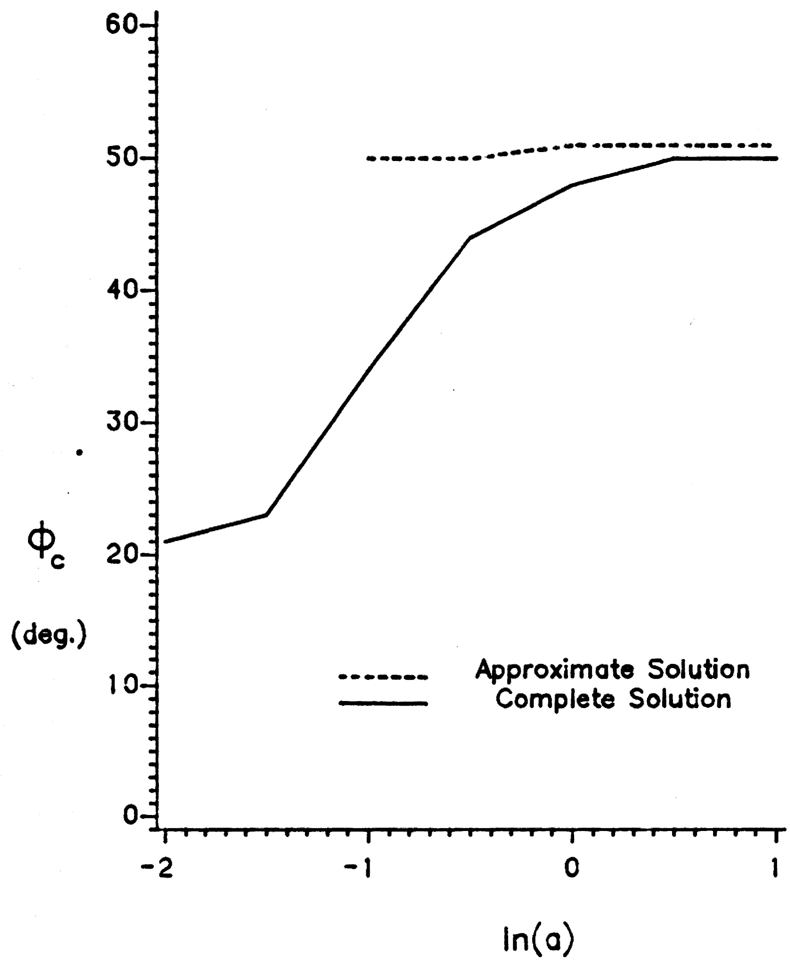

Fig. 3.6 Critical Angle (ϕ_c) Predicted by the Tensor Polynomial Theory Versus the Half Crack Length a

where W is the strain energy density:

$$W = \sum_{i=1}^{6} \sigma_i \varepsilon_i \qquad (3.6)$$

and r the distance from the crack tip. The elastic solution assumed here involves only the singular terms, therefore S is a function of ϕ only. The theory predicts crack extension at an angle corresponding to a local minimum (extremum) of S. The value S_c of S at this location is a characteristic of the material.

The results obtained for isotropic materials suggest choosing the highest minimum.

A typical strain energy density curve is given in Fig. 4.9 in the next chapter.

3.2.2 Role of the Parameters

For a perfectly elastic material, only the elastic constants and the far-field loading play a role in the prediction of ϕ_c, as they are the only parameters involved in the expression of the strain energy density. The loading at failure depends on only one toughness parameter, S_c.

3.2.3 Typical Results for Crack Growth Direction Prediction

Curves showing ϕ_c as a function of the fiber orientation for T300/5208 Gr/Ep under simple tension and simple shear are given in Fig. 3.7. Similar to the tensor polynomial theory, one should note that:

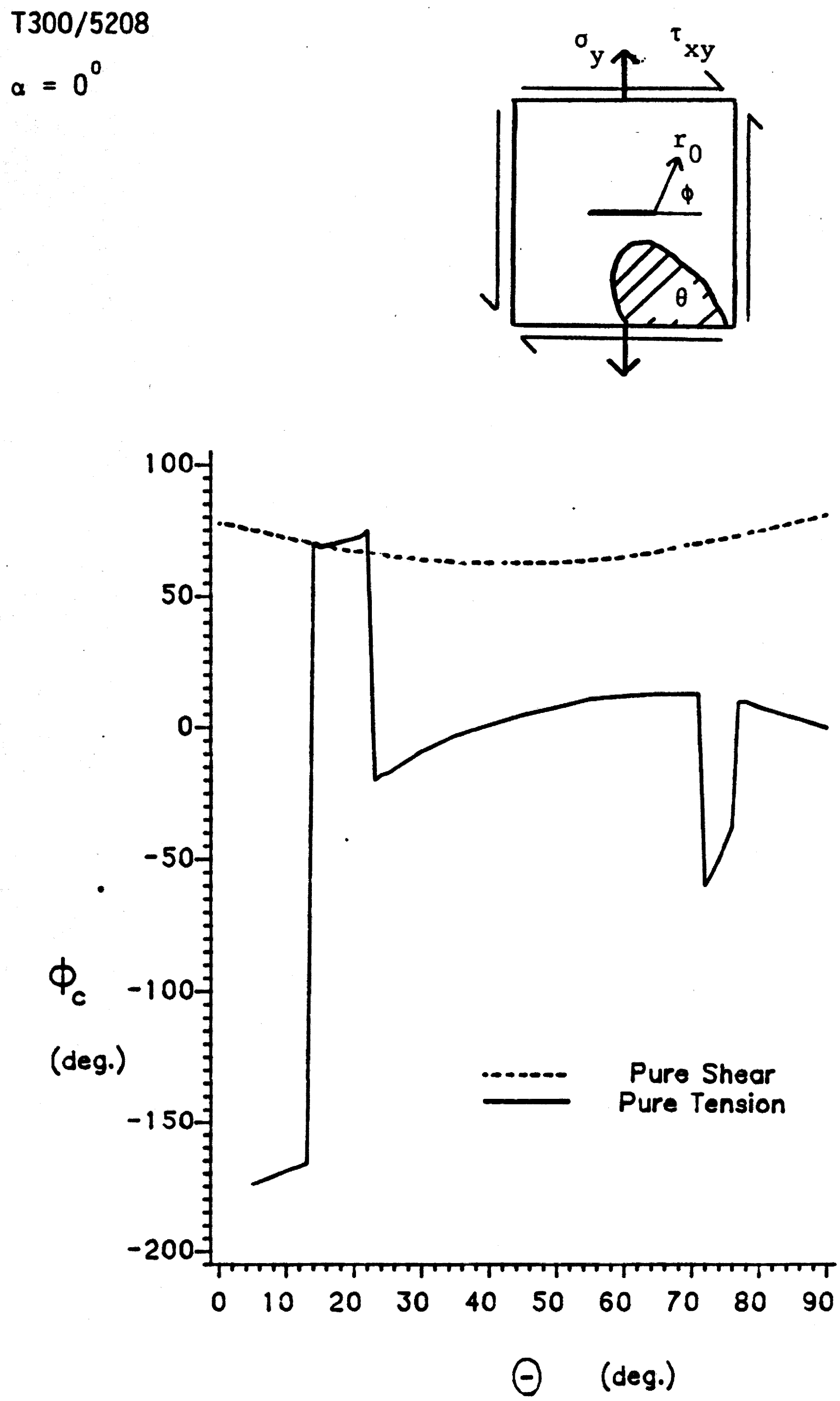

Fig. 3.7 Critical Angle (ϕ_c) Predicted by the Strain Energy Density Theory Versus the Fiber Orientation (θ)

- for a crack perpendicular to the fibers ($\theta = 90^0$), the theory predicts a self-similar propagation, or close to it.
- for a crack parallel to the fibers, the strain energy density factor shows no minimum except on the crack surface $\phi = \pm 180$, see Fig. 3.8). The strain energy density theory does not predict any direction of crack propagation in this case.

For the second case ($\theta = 0$), another interesting result can be observed. If the material considered is AS4/3501-6, the theory predicts propagation at an angle of 41° from the initial crack direction. This is illustrated by the plotting of S versus ϕ for AS4/3501-6 Gr/Ep, showing a local minimum at $\phi = 41°$ (Fig. 3.9).

The results obtained for $\theta = 0$ are contrary to experimental observation. There is no adjustable parameter that can be used to modify this prediction. These results illustrate the dependence of crack propagation direction on the material anisotropy.

Sih [3] uses an alternative approach in this theory by computing the strain energy density factor in the matrix only. By formulating the problem as a three phase model, Sih predicts a self similar propagation in the case of glass-epoxy.

3.3.0 Normal Stress Ratio

3.3.1 Presentation of the Theory

Buczek and Herakovich [14] have hypothesized the normal stress

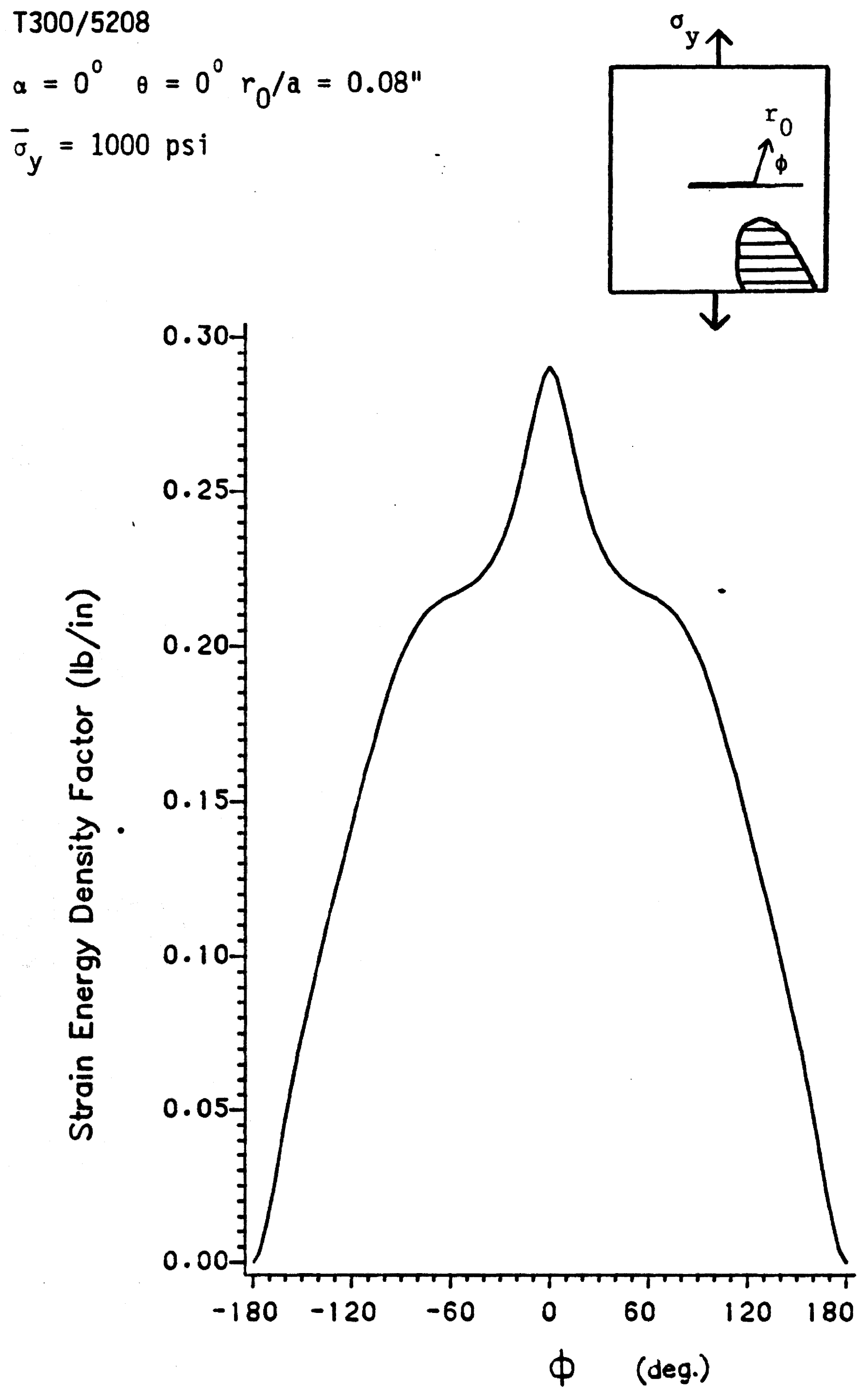

Fig. 3.8 Strain Energy Density Factor Versus Angle ϕ

AS4/3501-6

$\alpha = 0^0$, $\theta = 0^0$, $r_0/a = 0.08"$

$\bar{\sigma}_y = 1000$ psi

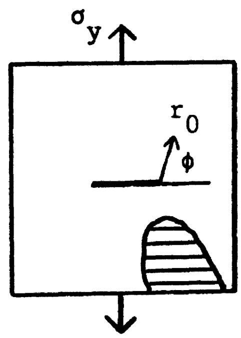

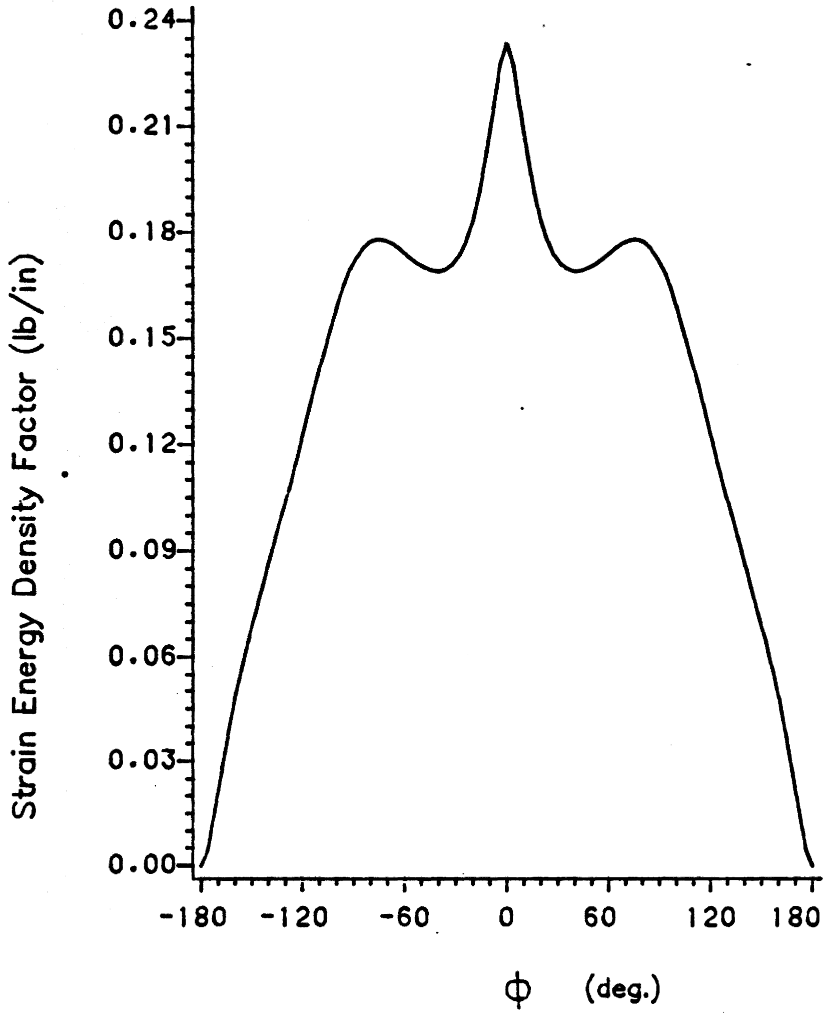

Fig. 3.9 Strain Energy Density Factor Versus Angle ϕ

ratio to be a phenomenological criterion for predicting the direction of crack growth. This quantity is defined as the ratio of the normal stress acting on a radial plane defined by ϕ and the tensile strength normal to this plane:

$$R = \frac{\sigma_{\phi\phi}}{T_{\phi\phi}} \tag{3.7}$$

Since the tensile strength of an arbitrary plane is generally unknown, a certain form of the function $T_{\phi\phi}$ has been hypothesized. The basic requirements that this function should meet are:

- For an isotropic material, $T_{\phi\phi}$ must be independent of ϕ
- For a plane perpendicular to the fibers, $T_{\phi\phi}$ must equal the tensile strength X_t
- For a plane parallel to the fibers, $T_{\phi\phi}$ must equal to the tensile strength Y_t

In the view above, $T_{\phi\phi}$ was chosen as

$$T_{\phi\phi} = X_t \sin^2\beta + Y_t \cos^2\beta \tag{3.8}$$

β being the angle between the radial plane defined by ϕ and the fiber direction θ (Fig. 3.10).

3.3.2 Role of the Parameters

The normal stress ratio can be computed at any distance from the crack tip. The results obtained for the crack propagation direction

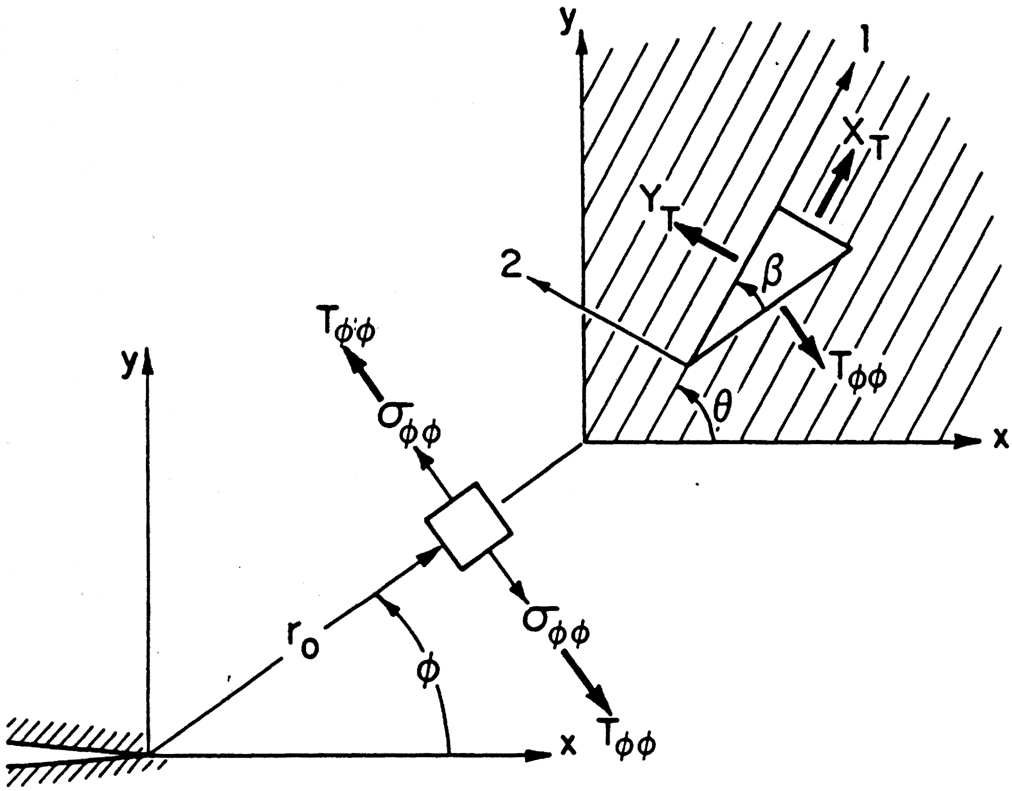

Fig. 3.10: Normal Stress Ratio Parameters

will depend on the distance r_0 only if the non-singular terms are taken into account in the elastic solution. In a reasonable range of variation of r_0, this dependence is very small. Fig. 3.11 shows the variation of ϕ_c, for a broad range of values of r, in the case of pure tensile load and fibers perpendicular to the crack. r_0 must be greater than the half crack length in order that ϕ_c deviates by more than 34° from the prediction obtained with the approximate solution.

3.3.3 Typical Results for Crack Growth Direction

Two curves showing the predicted angle of propagation versus the fiber angle for a pure tensile loading and a simple shear loading are given in Fig. 3.12. It can be seen that, for pure tensile loading:

- For a crack parallel to the fibers, this theory predicts self-similar propagation, as observed in experiments.
- For crack perpendicular to the fibers the theory predicts a propagation at an angle very close to the fiber direction, i.e. the theory predicts that matrix cracks occur before any fiber failure.

For pure shear loading, the theory predicts fiber fouline for a load range of values of θ (10° to 90°).

3.4.0 Traction Ratio

Presentation of the Theory

The normal stress ratio has been used only to predict the

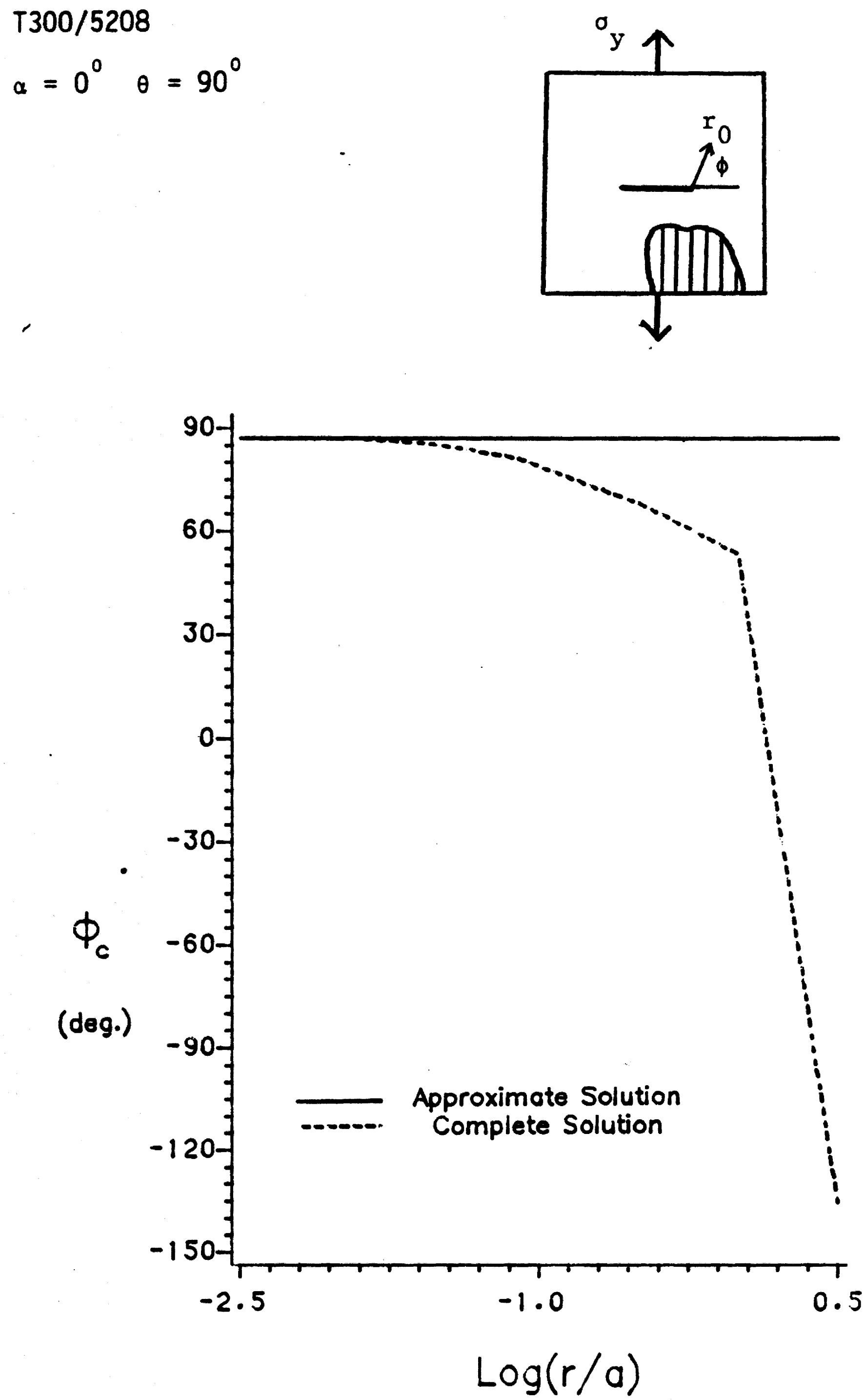

Fig. 3.11 Critical Angle (ϕ_c) Predicted by the Normal Stress Ratio Theory Versus r_0

T300/5208

$\alpha = 0^0$

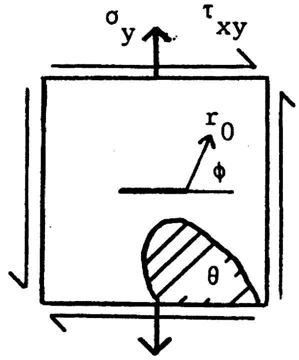

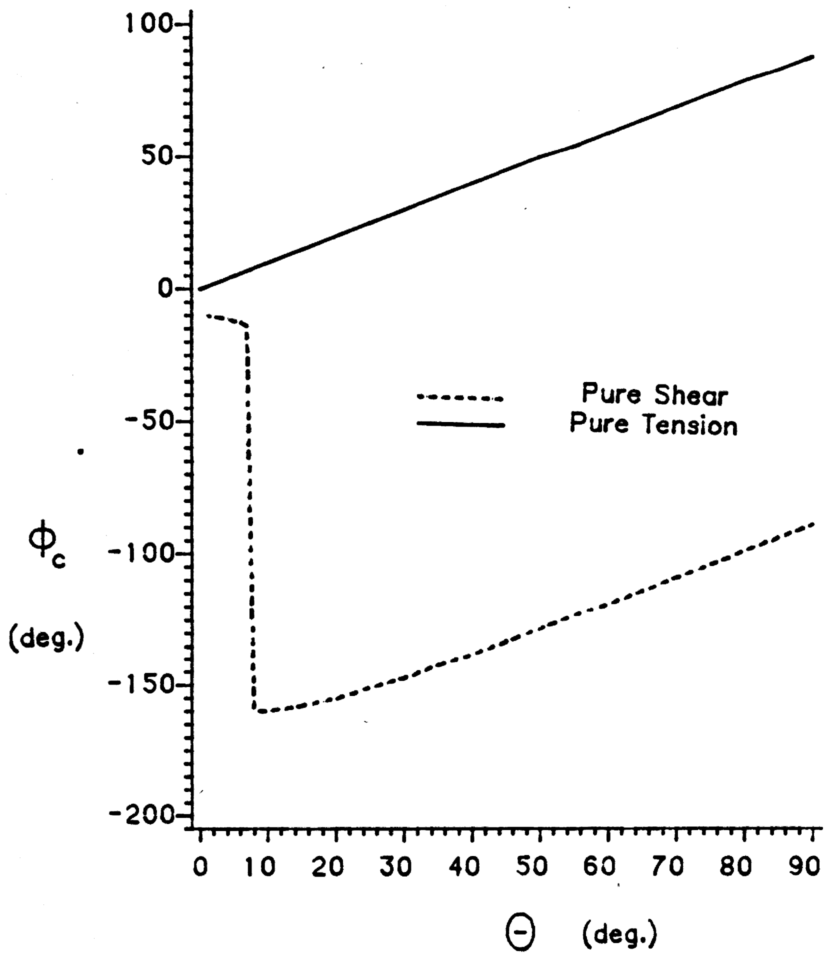

Fig. 3.12 Critical Angle (ϕ_c) Predicted by the Normal Stress Ratio Theory Versus the Fiber Orientation (θ)

direction of crack extension. It is desirable to have a theory which predicts both the critical load and the critical direction. Thus a new model based upon a traction ratio is presented here to predict the critical load for crack extension. This ratio TR is defined as:

$$TR = \frac{\Sigma}{\Lambda} \tag{3.9}$$

Σ being the magnitude of the traction vector acting on a radial plane defined by the angle ϕ and Λ being the amplitude of the traction resistance vector of this plane in the direction of the applied traction vector (Fig. 3.12).

The traction ratio factor TF is defined as:

$$TR = \frac{TF}{\sqrt{r}} \tag{3.10}$$

The propagation of the crack is hypothesized to occur when the maximum of TF reaches a certain value characteristic of the material, TF_c. The angle where this maximum occurs is the predicted direction of propagation.

Similar to the normal stress ratio theory, Λ cannot be measured for any angle ϕ and any traction vector orientation, therefore a certain form of the function Λ has been assumed which meets the following requirements:

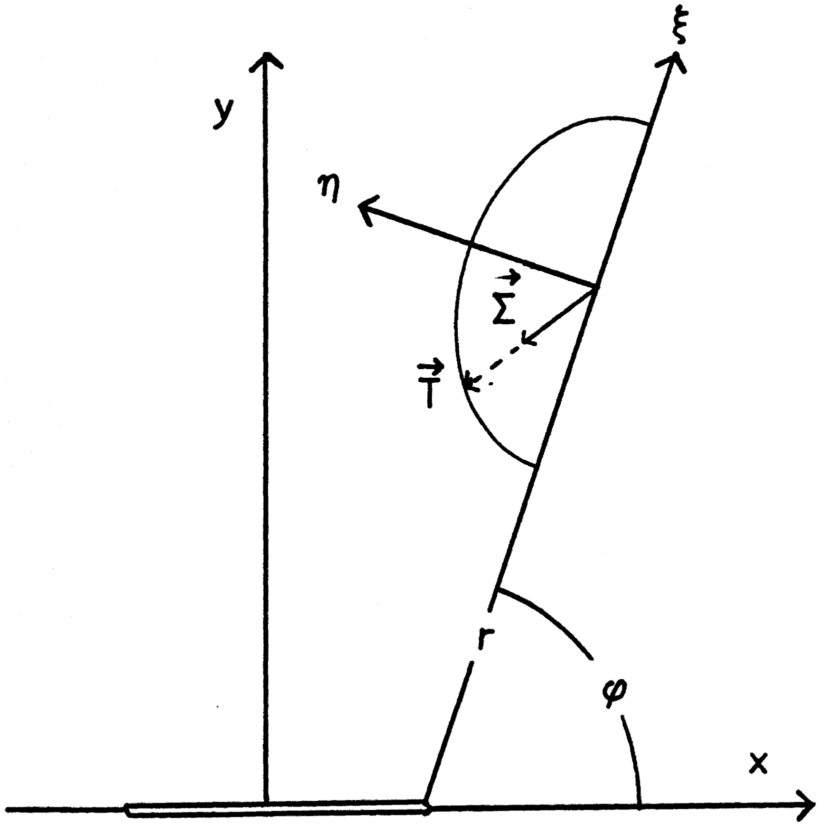

Fig. 3.13 Traction Ratio Parameters

- For a plane parallel to the fibers:

  Λ is equal to Y_t when the traction vector is normal to this plane.

  Λ is equal to S when the traction vector is parallel to this plane.

- For a plane perpendicular to the fibers, Λ must be equal to X_t when the traction vector is normal to the considered plane.

The resistance of a plane perpendicular to the fibers to pure shear is difficult to define, as a simple shear loading would most probably not fail this plane, but the one perpendicular to it. However, a certain interaction between normal and shear loading should exist, but it would be very difficult in fracture. Therefore, the resistance of a plane perpendicular to the fibers to a pure shear loading has been taken to be infinite.

In order to give explicitly the mathematical expression assumed for Λ, let us call ψ the angle between the traction vector and the considered plane (Fig. 3.13). For any plane the contour of the traction resistance vector has been assumed to be elliptic (Fig. 3.14). This is similar to Hashin's failure theory, [15]. The equation for Λ can be written as:

$$\Lambda = \left[\frac{\sin^2\psi}{A^2(\beta)} + \frac{\cos^2\psi}{B^2(\beta)} \right]^{-1/2} \qquad (3.11)$$

where $A(\beta)$ and $B(\beta)$ are the intersection of the contour with the η and ξ axis, respectively (Fig. 3.14).

For a plane parallel to the fibers, this ellipse intersects

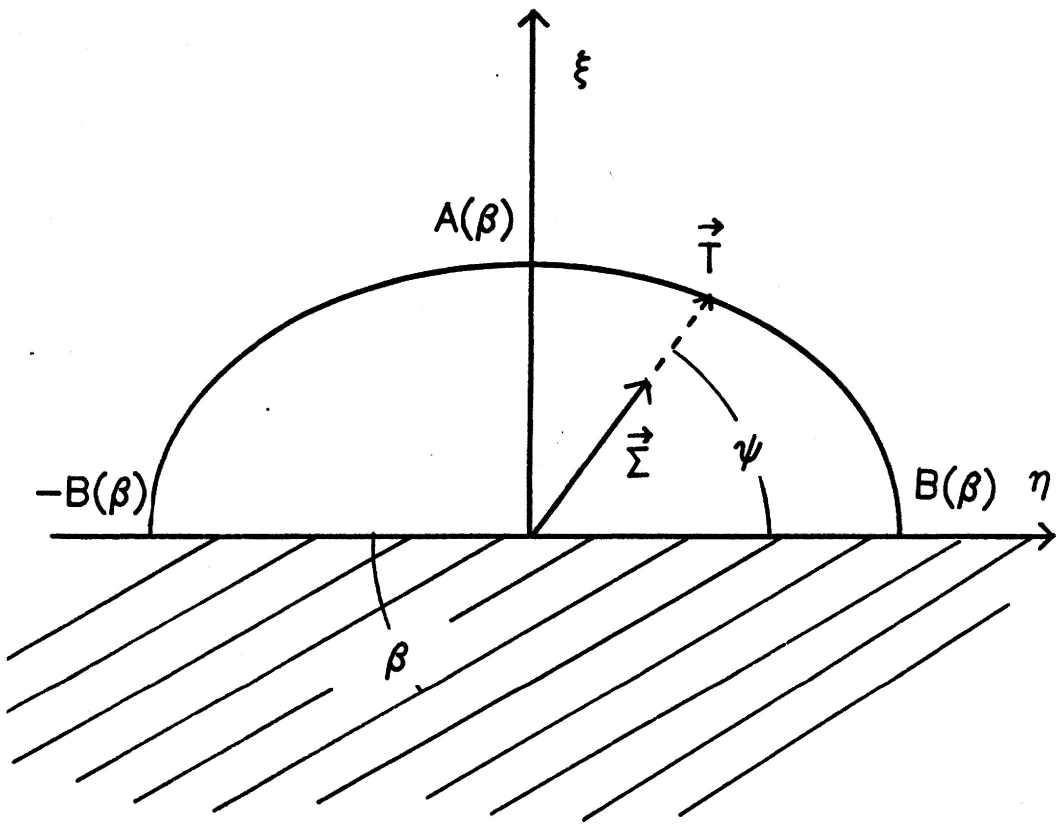

Fig. 3.14 Traction Vector and Traction Resistance Vector

the ξ and η axis at Y_t and S, respectively (Fig. 3.16). Therefore,

$$A(\beta = 0) = Y_t$$

$$B(\beta = 0) = S$$

For a plane perpendicular to the fibers, this ellipse degenerates into a right parallel to the considered plane (Fig. 3.16). Therefore,

$$A(\beta = 90) = X_t$$

$$B(\beta = 90) = \infty$$

The functions A and B are then taken to be of the forms:

- $A(\beta) = X_t \sin^2(\beta) + Y_t \cos^2(\beta)$

- $B(\beta) = S(1 + \tan(\beta))$ (3.12)

It has been also hypothesized that failure does not occur in the directions where the traction vector corresponds to a compressive state of normal stress. Therefore the traction ratio should have the same sign as the normal stress.

3.4.2 Influence of r_o

Similarly to the normal stress ratio theory, the results for crack direction and load at failure are independent of r_o if only the

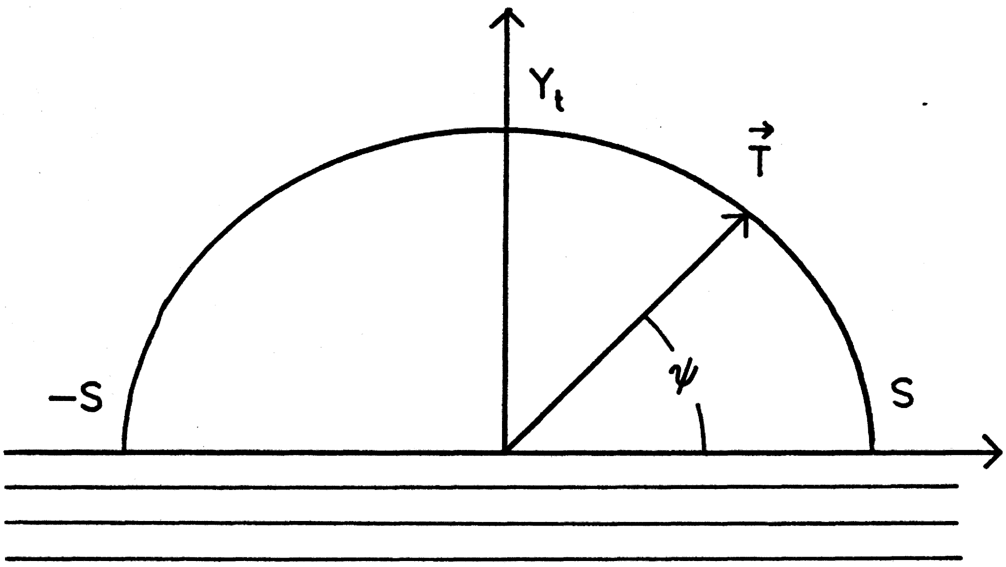

Fig. 3.15: Traction Vector and Traction Resistance Vector for a Plane Parallel to the Fibers

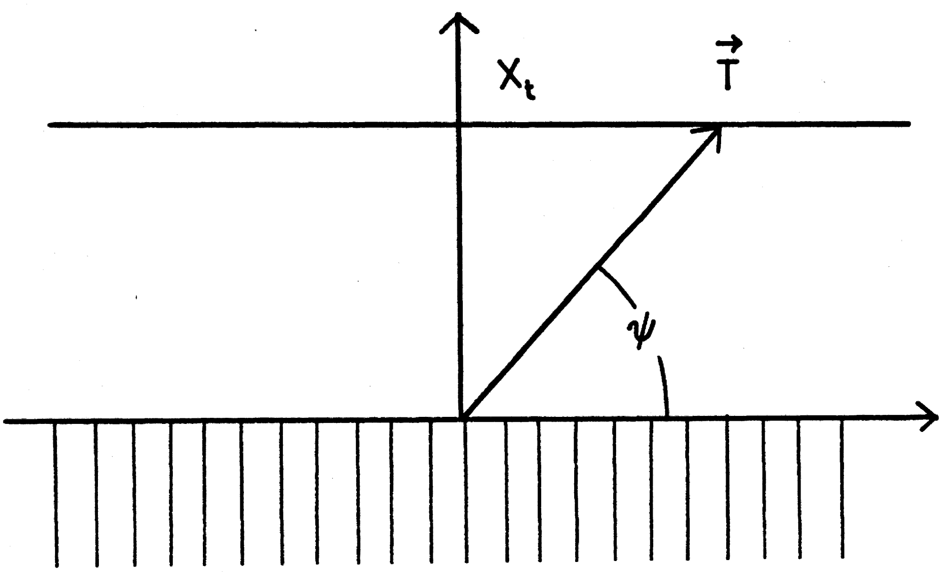

Fig. 3.16 Traction Vector and Traction Resistance Vector for a Plane Perpendicular to the Fibers

singular terms in the stress functions are taken into account. This is the approach chosen here.

3.4.3 Typical Results for Crack Growth Direction Prediction

Curves showing the predicted angle of crack extension as a function of the fiber orientation for pure normal and simple shear loadings are given in Fig. 3.17. The results are similar to those of the normal stress ratio theory. However, the traction ratio predicts self-similar propagation ($\phi_C = 0^0$) for a crack parallel to the fibers subjected to a simple shear loading. The normal stress ratio predicted -10° in the example given in Fig. 3.12.

3.5 Role of the Material Anisotropy

It has been found that, contrary to the isotropic case, when a pure tensile load is applied the predicted direction of crack growth differs from self-similar growth in the following situations:

- For the traction ratio and normal stress ratio when the fibers are perpendicular to the crack and parallel to the loading (Fig. 3.12 and 3.17).
- For the strain energy density and the tensor polynomial when the fibers are parallel to the crack and perpendicular to the loading (Fig. 3.3 and 3.7).

It is interesting to know how the degree of anisotropy affects the predictions and also to classify the criteria with respect to their sensitivity to material anisotropy. This can be done by varying

T300/5208

$\alpha = 0^{0}$

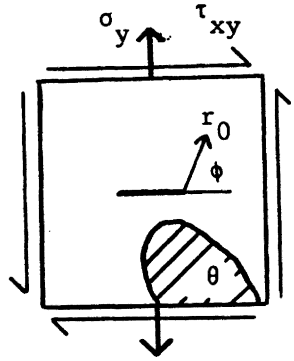

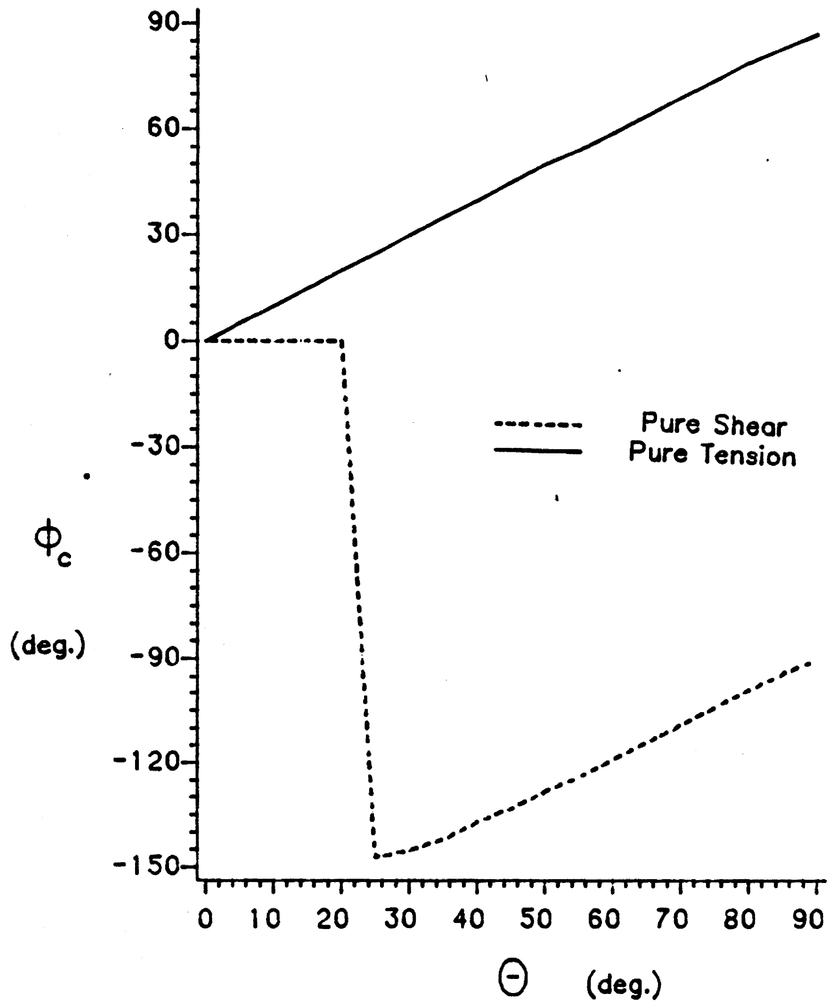

Fig. 3.17 Critical Angle (ϕ_C) Predicted by the Traction Ratio Theory Versus the Fiber Orientation (θ)

the percentage of fibers in a composite and plotting the predicted angle of propagation versus a parameter measuring the degree of anisotropy.

This has been done by using the rule of mixtures for computing the elastic constants of the composite as a function of the volume fraction. If the subscript f indicates the fibers and the subscript m indicates the matrix, then, from the rule of mixtures,

$$
\begin{aligned}
&\cdot\ E_1 = V_f E_f + (1 - V_f) E_m \\
&\cdot\ 1/E_2 = \frac{V_f}{E_f} + \frac{V_m}{E_m} \qquad (3.13) \\
&\cdot\ \nu_{12} = V_f \nu_f + (1 - V_f) \nu_m \\
&\cdot\ 1/G_{12} = \frac{V_f}{G_f} + \frac{V_m}{G_m}
\end{aligned}
$$

The strength constants are more difficult to estimate. If we suppose that the composite breaks when the fibers break, then X_t can be evaluated by [16]:

$$X_t = V_f X_f + (1 - V_f)(\sigma_m) \text{ at } \sigma_f = \sigma_u \qquad (3.14a)$$

σ_u being the ultimate stress for the fibers.

This formula is meaningful when V_f is not too small, but does not converge to the isotropic case when V_f approaches zero.

X_c has been taken as $-X_t$, and the variations with V_f of Y_t, Y_c

and S have been neglected, i.e.:

$$Y_t = -Y_c = X_m \qquad (3.14b)$$

$$S = S_m$$

The physical properties of the matrix and the fibers (E_f, ν_f, X_f, E_m, ν_m, X_m) have been chosen such that the properties of T300 Gr/Ep are obtained exactly for the volume fraction corresponding to this material, estimated at 62%.

The nine functions of V_f obtained may not represent well the actual situation when the fiber volume fraction is far from 62%, but only a rough estimate is needed here, as too many other parameters are also involved. The parameter p measuring the anisotropy has been chosen as E_1/E_2. It should be noted that its variation versus V_f is not monotonic when V_f is close to 60% (see Fig. 3.18).

Two curves giving ϕ_c versus p for all the four theories are given in Fig. 3.18 and 3.19, for pure tensile load and with fibers perpendicular ($\theta = 90^0$) and parallel ($\theta = 0^0$) to the loading, respectively.

For $\theta = 90^0$ (Fig. 3.18), the normal stress ratio and traction ratio show a strong and similar sensitivity for weak anisotropy, and give relatively stable results for high anisotropy. The strain energy density theory predicts self-similar propagation when E_1/E_2 is low. The prediction deviates from self-similarity around p = 3, and stabilizes around 13° for high p.

For $\theta = 0^0$ (Fig. 3.19), the tensor polynomial appears to be the

AS4/3501-6

$\alpha = 0^0 \quad \theta = 90^0 \quad r_0/a = 0.01''$

$\bar{\sigma}_y = 1000$ psi

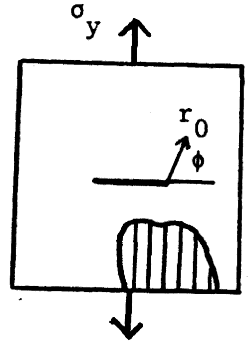

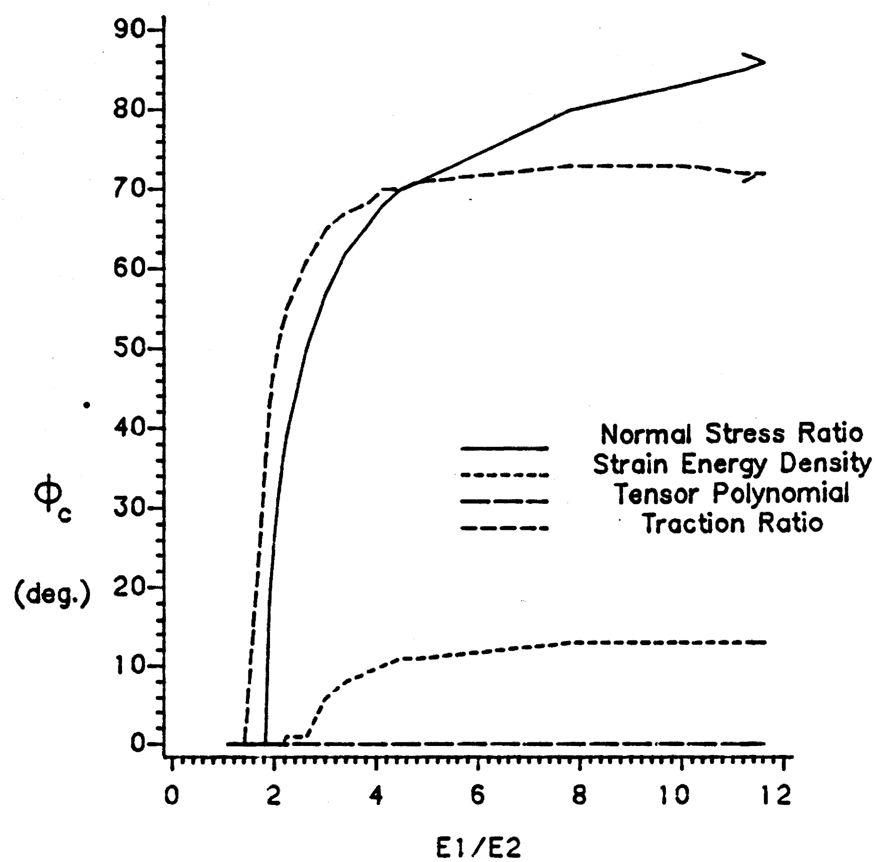

Fig. 3.18 Critical Angle (ϕ_c) Versus E_1/E_2

AS4/3501-6

$\alpha = 0^0 \quad \theta = 0^0 \quad r_0/a = 0.01"$

$\bar{\sigma}_y = 1000$ psi

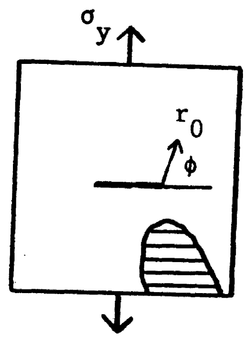

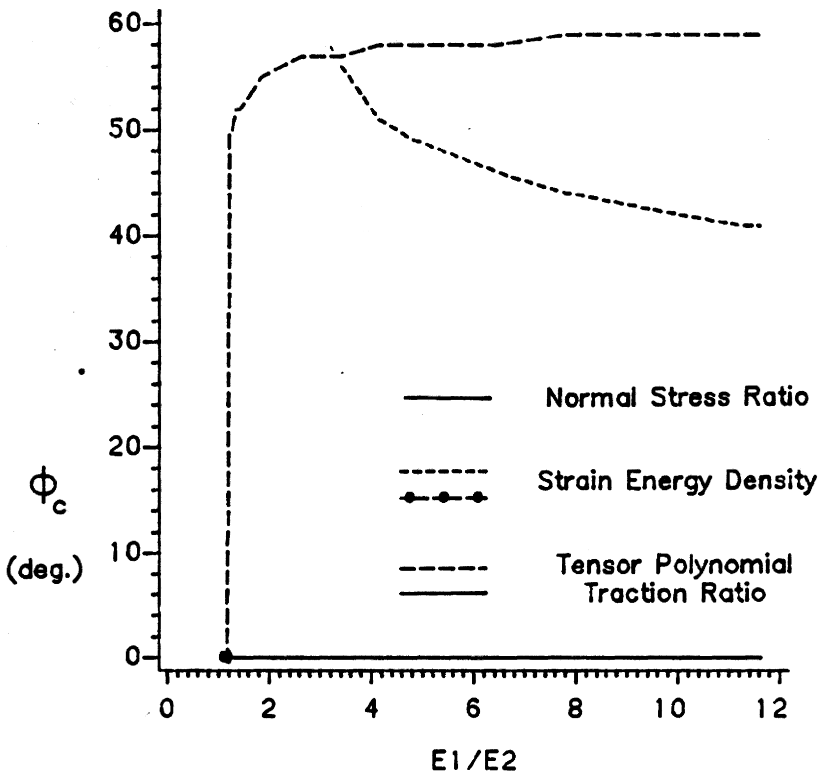

Fig. 3.19 Critical Angle (ϕ_c) Versus E_1/E_2

most sensitive to the anisotropy for low E_1/E_2, and rather insensitive for high anisotropy. The strain energy density prediction is $\phi_c = 0^0$ for weak anisotropy, and is less stable at high E_1/E_2. There is no prediction ($\phi_c = \pm 180^0$) between these two domains (see section 3.2.3). The normal stress ratio and traction ratio prediction is $\phi_c = 0^0$, independently of the degree of anisotropy.

Most advanced composite currently in use have a ratio E_1/E_2 greater than 3 and less than 12. The variation of predicted ϕ_c are small for any of the four criteria in this range of the above p values. Although it should be verified for fibers and matrix of other types, this indicates that ϕ_c is not a strong function of fiber volume fraction for typical materials currently in use.

4.0 Comparison of Theoretical Predictions and Experimental Results

4.1 Case of Single Mode Loading of Boron Aluminum

4.1.1 Description of the Experiments

Several experiments on the propagation of cracks in multi-layered boron-aluminum laminates have been conducted by C. C. Poe and J. A. Sova [9]. The four previously described theories will be applied in the case of four notched laminates made of six identical 0° plies.

A set of pictures [9] representing the cracked laminates for various initial notch lengths are reproduced in Fig. 4.1. It appears that the crack propagation includes self-similar fiber breakage and matrix cracks parallel to the fibers.

It is important to know whether the matrix crack or the fiber breakage occurred first. One specimen was carefully observed throughout the testing. It was reported [9] that matrix cracks appeared when the load exceeded about 93% of the failure load. These cracks were very small until failure.

4.1.2 Results with the Tensor Polynomial

The tensor polynomial theory is difficult to apply here. For any one of the 4 specimens studied, the distance r_0 has to be chosen of the same order as the half crack length in order that the maximum value of the tensor polynomial be 1. For such large r_0, the non-singular terms of the elastic solution are of the same magnitude as the singular terms. The characteristic value of r_0 which provides the

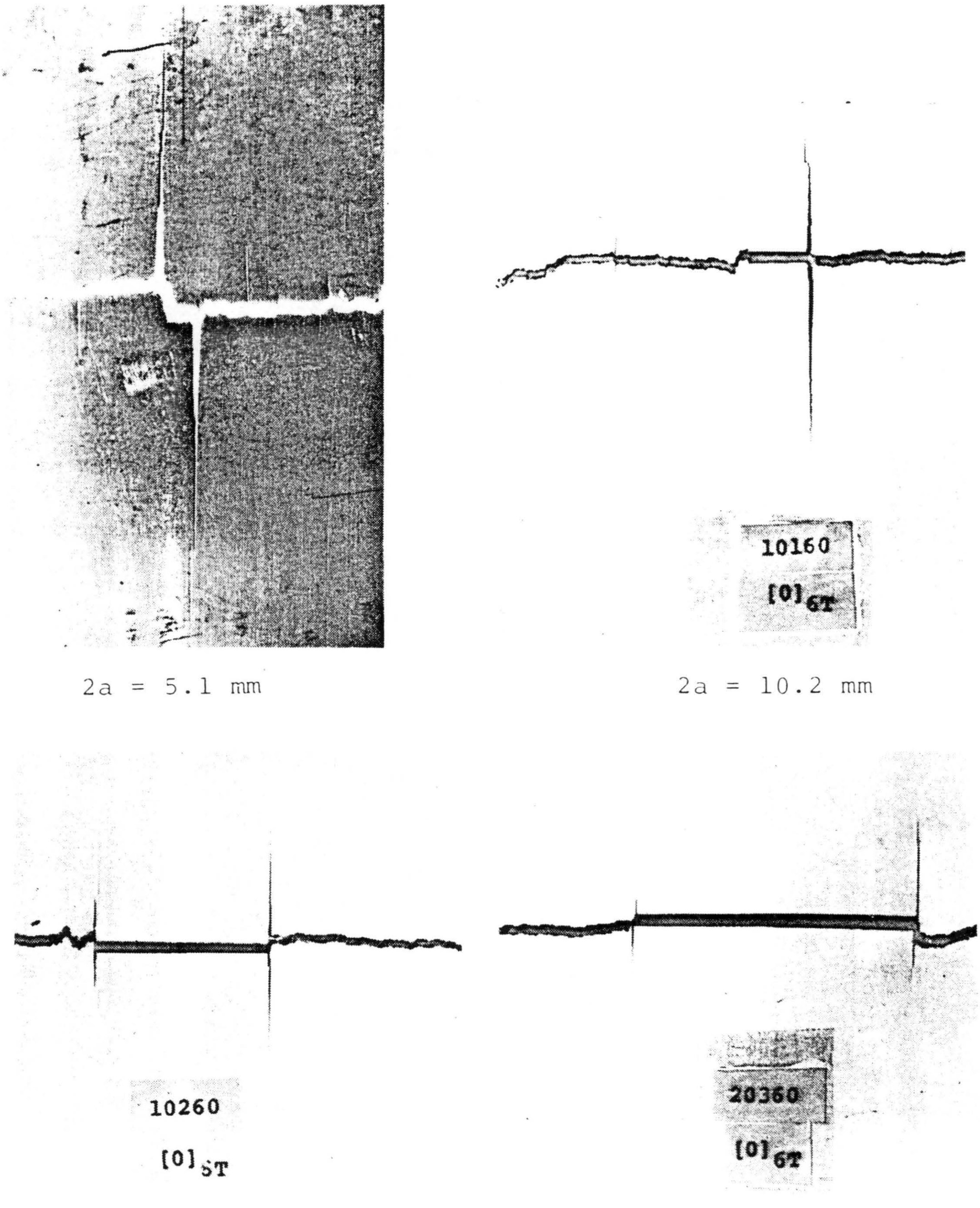

2a = 5.1 mm

2a = 10.2 mm

2a = 30.5 mm

2a = 50.8 mm

Fig. 4.1 Failed Specimens of Boron/Aluminum [9] best fit with experimental results is larger than the smallest crack length, and the maximum value of the tensor polynomial occurs away from $\phi = 0^0$. This is not the case when the singular terms only are taken into account. A plot of the tensor polynomial versus angle ϕ is given in Fig. 4.2 (solid line). r_0 is chosen as 0.0415", and the maximum value 1.0 is reached at $\phi = 180^0$. At this angle, the crack tip considered is farther from the point of analysis than the other crack tip, and therefore has less influence on the stress concentration. This theory does not seem to be applicable here, and this may be due to an underestimation of the strength constants. If the approximate solution is used the maximum value is reached at $\phi = 0^0$, which indeed corresponds to one of the two experimentally observed directions of propagation (Fig. 4.2, dotted line).

In this example, the tensor polynomial shows a high sensitivity to the values of the strength constants.

4.1.3 Strain Energy Density Results

As no data has been found for the characteristic value S_c for boron/aluminum, it has been chosen in order to minimize the difference between predicted values and experimental results (S_c = 4831, see Appendix A).

The direction of propagation predicted by this theory corresponds to fibers breakage. A set of curves given in Fig. 4.3 represents the strain energy density versus angle ϕ for the four samples and at the experimentally measured failure load. Each of the four curves shows

Boron/Aluminum

$\alpha = 0^{\circ}$ $\theta = 90^{\circ}$

$a = 15.25$ mm $r_0 = 41.5$ mm

Experimental load at failure

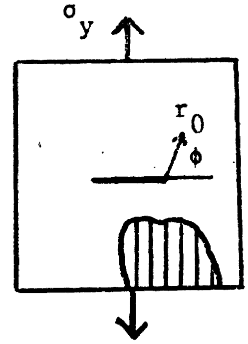

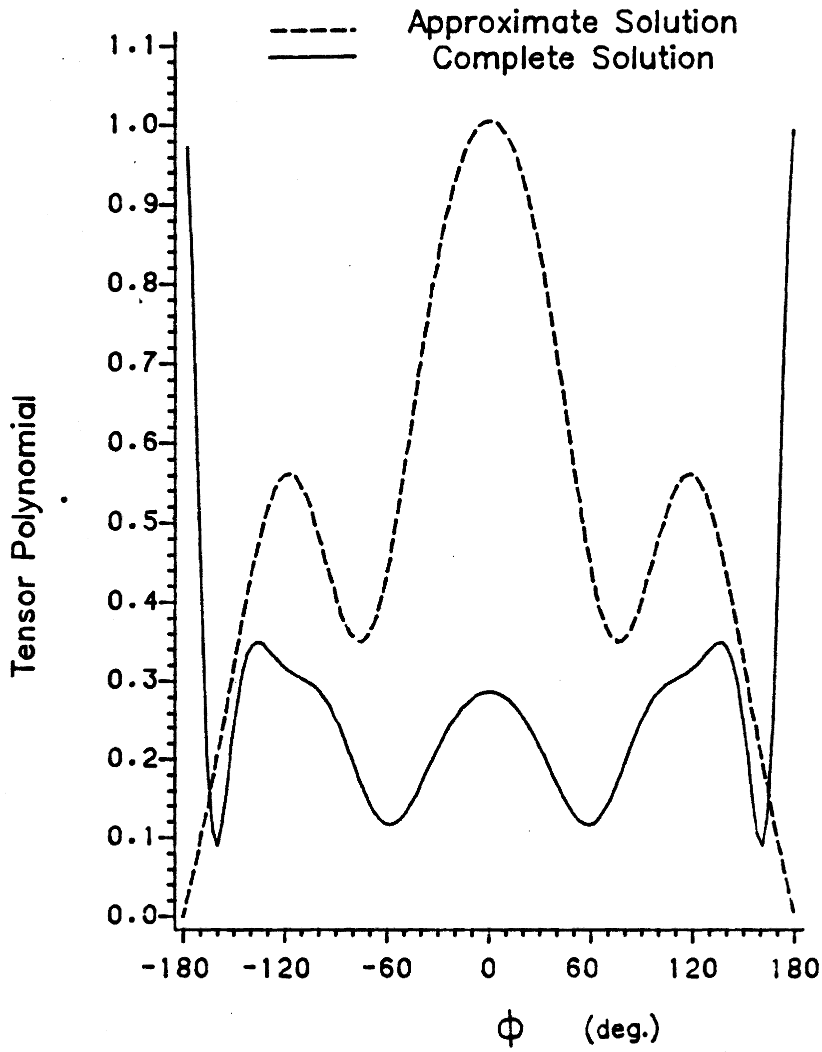

Fig. 4.2 Tensor Polynomial Versus Angle ϕ

its highest minimum at $\phi = 0^{0}$, which is the predicted direction of crack propagation.

In this case of mode one loading, if we use the approximate elastic solution,

$$\sigma_{i}(\phi = 0) = \bar{\sigma}_{y}(a/r)^{1/2} f(\phi = 0)$$

$$\varepsilon_{i}(\phi = 0) = \bar{\sigma}_{y}(a/r)^{1/2} g(\phi = 0) \tag{4.1}$$

σ being the applied stress, the strain energy density factor is

$$S = r\sigma_{i}\varepsilon_{i} = \bar{\sigma}_{y}^{2}\ a\ F(\phi = 0) = S_{c}$$

Therefore, the S.E.D. theory is analogous to the classical stress intensity factor theory, as at fracture initiaton we have:

$$\bar{\sigma}_{y}\sqrt{\bar{a}} = (S_{c}/F(\phi = 0))^{1/2} = K \tag{4.2}$$

The predicted loads at failure are given in Table 4.1.

4.1.4 Results with the Normal Stress Ratio

The plots of the normal stress ratio versus ϕ for each laminate are given in Fig. 4.4. The maxima of these curves are sharp, peak at the critical angles. The predicted direction of propagation is 87°, which seems to correspond to the matrix cracks observed in Fig. 4.1.

Boron/Aluminum

$\alpha = 0^0$ $\theta = 90^0$

Experimental loads at failure

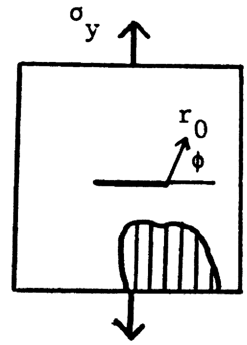

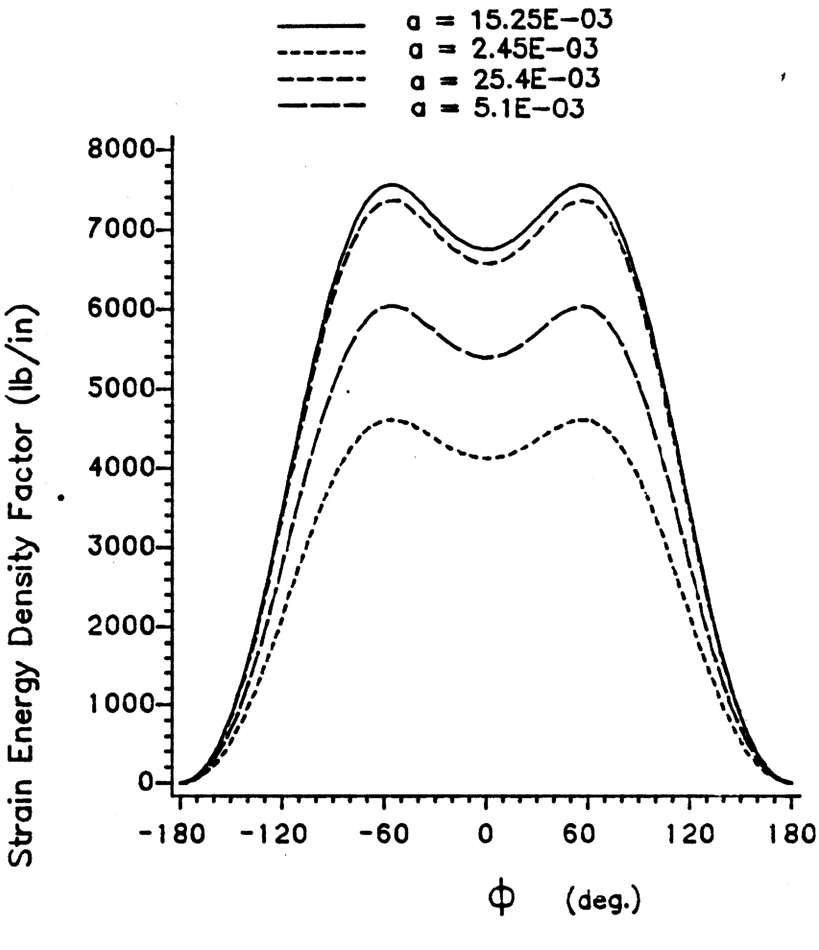

Fig. 4.3 Strain Energy Density Factor Versus Angle ϕ

Boron/Aluminum

$\alpha = 0^0 \quad \theta = 90^0$

Experimental loads at failure

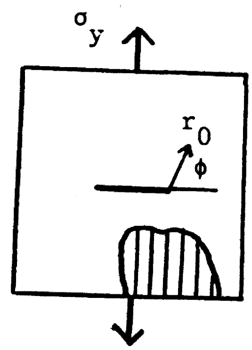

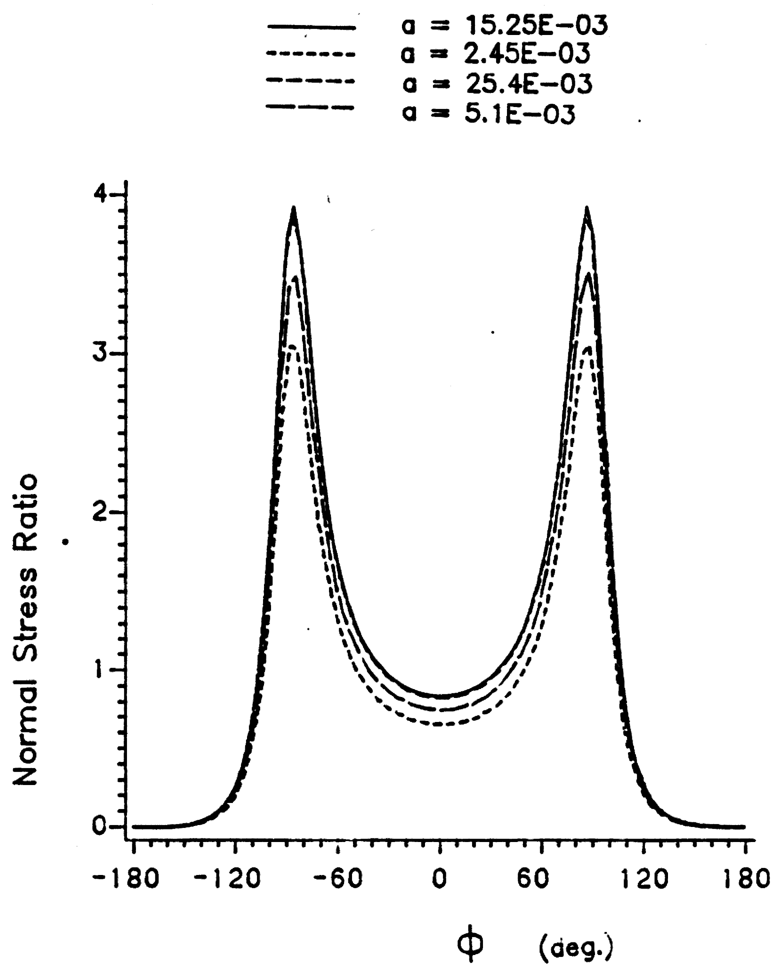

Fig. 4.4 Normal Stress Ratio Versus Angle ϕ

4.1.5 Results with the Traction Ratio

The traction ratio curves for the four laminates and the experimentally determined load at failure are given in Fig. 4.5. The value of TF_c used here is 0.129 (see Appendix A). The predicted angle of propagation corresponds also to the matrix crack (87°), as was the case for the normal stress ratio.

In this case the angle which maximizes the traction ratio is independent of r_o. As the approximate elastic solution has been used we can write (ϕ_c being the predicted angle of propagation):

$$\sigma_i(\phi_c) = \bar{\sigma}_y(a/r)^{1/2}f(\phi_c) \tag{4.3}$$

The angle ξ between the plane oriented at angle ϕ and the traction vector is independent of a, so for any given angle ϕ, Λ is the same for all specimens. Therefore the traction ratio theory gives:

$$\sqrt{r}\Sigma/T = \bar{\sigma}_y(a)^{1/2}F(\phi_c) = TF_c \tag{4.4}$$

As for the SED theory, this is equivalent to the stress intensity factor theory. Therefore, the SED and the traction ratio theories must give the same results for the loading. The results are given in Table 4.1.

4.1.6 Conclusion

The two modes of failure observed in Fig. 4.1 are predicted each

Boron/Aluminum

$\alpha = 0^{0}$ $\theta = 90^{0}$

Experimental loads at failure

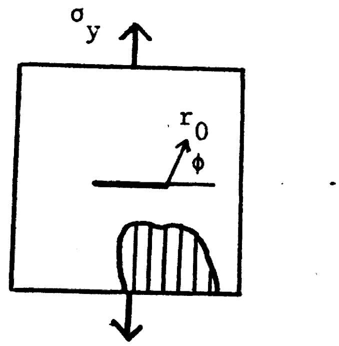

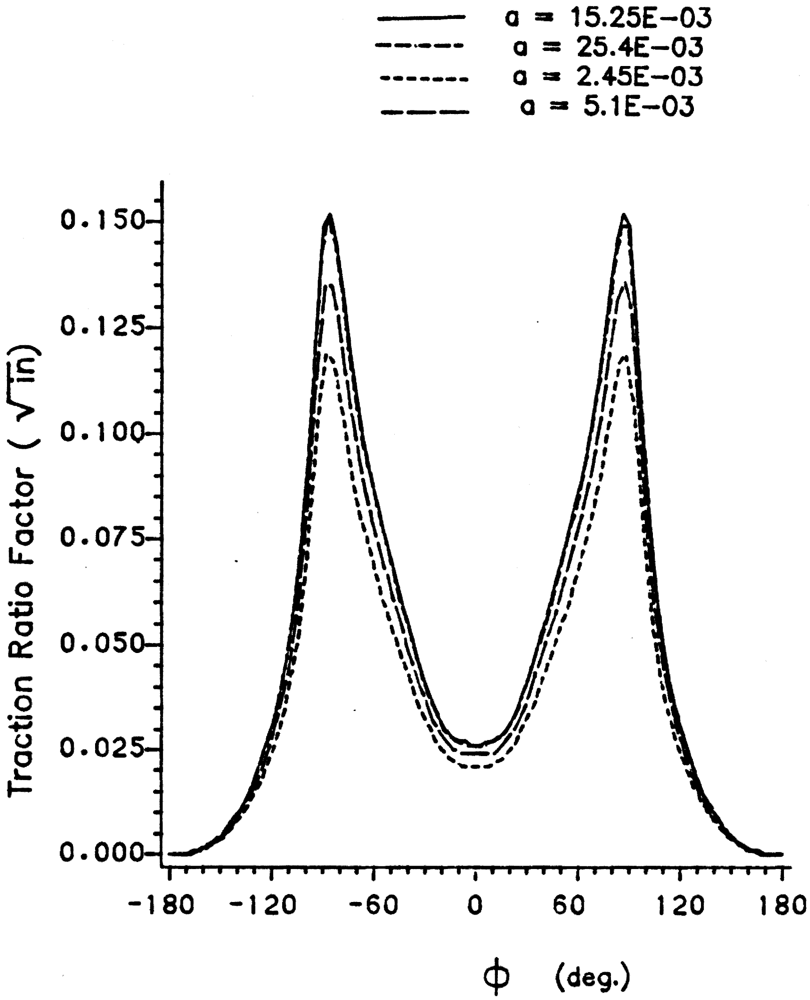

Fig. 4.5 Traction Ratio Versus Angle ϕ

one by one or two of the four criteria studied here. It is not clearly known which one has occured first. However, if the crack had extended first across the fibers, the stress intensity in the vicinity of the initial notch would have been relieved, and there is no sufficient reason why the matrix should fail in this region. Therefore, the matrix cracks have more likely appeared first, which supports the normal stress ratio and traction ratio theories.

As far as the critical load prediction is concerned, only the strain energy density and the traction ratio can be used. They give identical results. It is interesting to note that the predicted load at failure is too high for small a and too low for large a. This could be corrected by using the complete elastic solution and computing the traction ratio or the strain energy density at a certain fixed distance r_0 from the crack tip. This could indicate that the non-singular stresses play a role in the fracture propagation. However, the initial notches are far from an ideal crack shape, and this may also play an important role so that this conclusion may not be drawn with confidence. A plot of the predicted and experimental loads at failure versus the half crack length a is given in Fig. 4.6. The results were obtained with the traction ratio, using the approximate elastic solution, and the complete elastic solution with r_0 = 0.0015 mm. The complete solution predicts critical loads very close to the experimental results.

Table 4.1 Experimental and Predicted Load at Failure and Direction of Crack Extension for Boron/Aluminium.

a	Normal Stress Ratio		Strain Energy Density		Traction Ratio		Experimental	
	σ_y	ϕ_c	σ_y	ϕ_c	σ_y	ϕ_c	σ_y	ϕ_c
2.54		87°	1048	0°	1048	87°	969	0° 90°
5.1		87°	740	0°	740	87°	782	0° 90°
15.25		87°	428	0°	428	87°	506	0° 90°
25.4		87°	331	0°	331	87°	387	0° 90°

The loads σ_y are in psi.

The half crack length a is in millimeters.

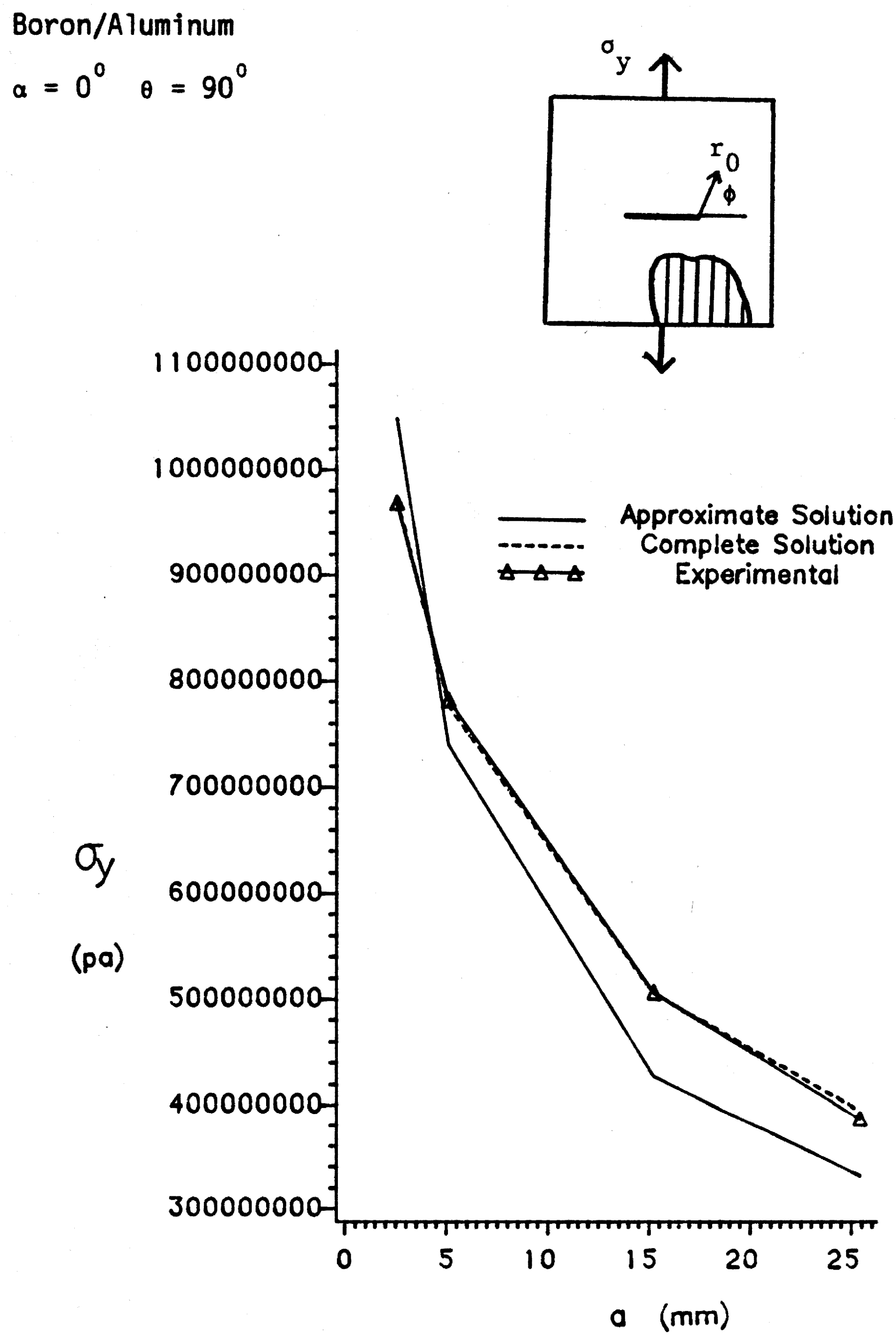

Fig. 4.6 Critical Load (σ_y) Predicted by the Traction Ratio Theory Versus the Half Crack Length (a) Using the Approximate and the Complete Solutions.

4.2 A case of Mixed Mode of Loading for Gr/Ep

4.2.1 Description of the Experiments

Several off-axis notched specimen of Gr/Ep have been tested by Herakovich, Gregory and Beuth [17]. A series of six 15° off-axis specimens with varying aspect ratios and pre-machined cracks oriented perpendicular to the loading direction or perpendicular to the fibers were tested in a testing machine with rigid end constraints. The specimens failed are shown in Fig. 4.7. As shown by Pagano and Halpin [18], the remote stress field includes a shear component, depending on the aspect ratio of the specimen. Therefore, three different case of mixed-mode loading are obtained.

4.2.2 Experimental Results

Table 4.2 gives the initiation load, the failure load, and the direction of propagation of the crack for each case. If the specimens with a crack perpendicular to the fibers are designed by A, and those with a crack perpendicular to the loading are designed by H, it appears that:

- The crack always propagates parallel to the fibers.
- The scatter in the critical load between two identical specimen is quite large in the H case and much less in the A case.
- No trend in the value of the stress causing initial crack growth with respect to the aspect ratio is apparent.

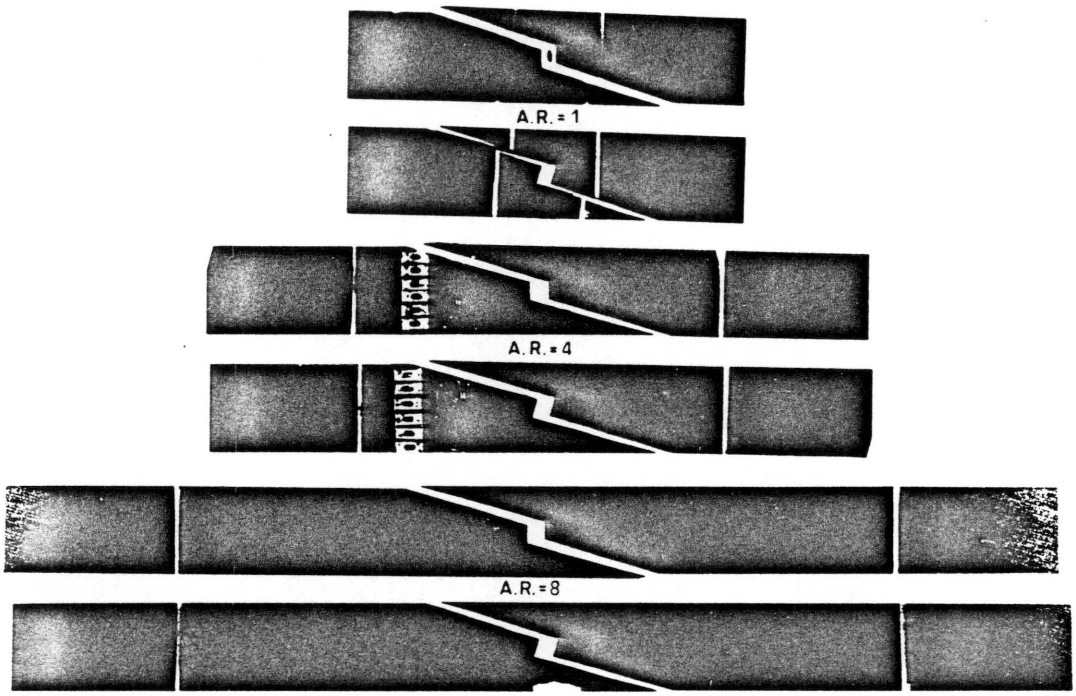

Fig. 4.7 Failed Test Specimen of 15° Off-Axis AS4/3501-6

- The load causing crack initiation shows a tendency to be higher in the case H.

4.2.3 Comparison Between Theories and Experiments

In order to compare the predicted critical load σ_y^p with the experimental values σ_y^e, two quantities A_1 and A_2 have been defined for the tensor polynomial, the strain energy density and the traction ratio criteria.

$$A_1 = \Sigma(\sigma_y^p - \sigma_y^e)^2$$

$$A_2 = \sum_{\substack{\text{aspect}\\ \text{ratio}}} \left(\frac{\sigma_y^p\ (\alpha = -15^\circ)}{\sigma_y^p\ (\alpha = 0^\circ)} - \frac{\sigma_y^e\ (\alpha = -15^\circ)}{\sigma_y^e(\alpha = 0^\circ)} \right)^2 \tag{4.5}$$

The value of A_1 is a measure of the global deviation from experimental results. A_2 measures the correlation with the experimetally observed tendency of the loading to be higher when $\alpha = 0^\circ$ than when $\alpha = -15^\circ$.

4.2.4 Results with Tensor Polynomial

The radius r_0 giving the best results for the prediction of the critical load is 0.0029" (see Appendix A). The results obtained are summarized in Table 4.2, and a plot of the contour of the stress vector and the strength vector of one case is given in Fig. 4.8. It can be seen that these two curves are very close over a rather large sector containing the critical angle. Therefore a slight variation in

AS4/33501-6

$\alpha = -15.^{\circ}$ $\theta = 75.^{\circ}$

$a = 0.1"$ $r_0 = 0.0029"$

Predicted load at failure

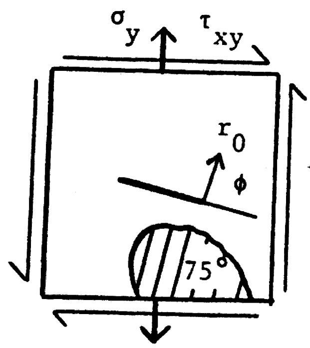

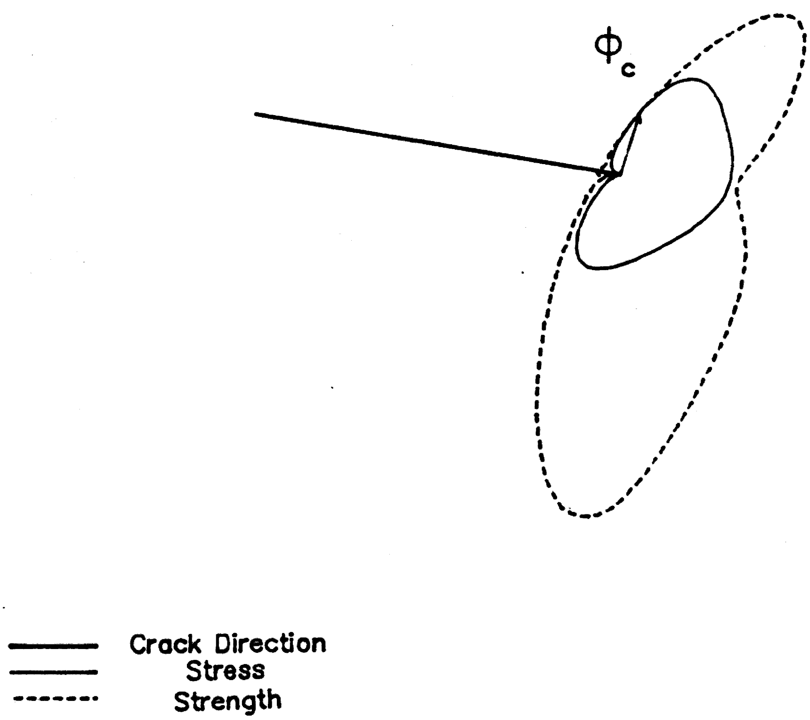

Fig. 4.8 Contour of the Stress and Strength Vector (specimen with an aspect ratio of 1)

the stress vector can cause significant variations in the predicted angle of crack extension.

The predicted direction of crack propagation is fairly correct, except in one case (specimen with an aspect ratio of γ and a crck angle of -15°). The predicted load at failure shows a high sensitivity to the aspect ratio. This is not evident in the experimental results (A_1 = 1.83 10^7 psi^2). This criteria does provide the best representation of the tendency of the specimens with $\alpha = 0^0$ to fail at higher loads than the specimens with $\alpha = -15^0$ (A_2 = 0.34).

4.2.5 Results with Strain Energy Density

The results given by the strain energy density theory are given in Table 4.2. A plot of the strain energy density factor for the case 1A is reproduced in Fig. 4.8. The predicted angle is rather far from the fiber direction. The maximum of the strain energy density factor occurs closer (and sometimes very close) to the correct prediction than the relative minimum the theory prescribes.

The material constant S_c has been chosen in order to minimize the difference between the predicted and the experiemntal results for the criterial load. The strain energy density criteria gives the closest results to the experimental data (A_1 = 0.62 10^7 psi^2). Howver, the influence of the angle α is poorly or totally not represented (A_2 = 0.078).

AS4/3501-6

$\alpha = -15.^{0}$ $\theta = 75.^{0}$

$a = 0.1"$ $r_0 = 0.0029"$

Predicted load at failure

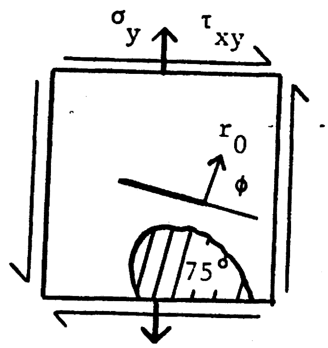

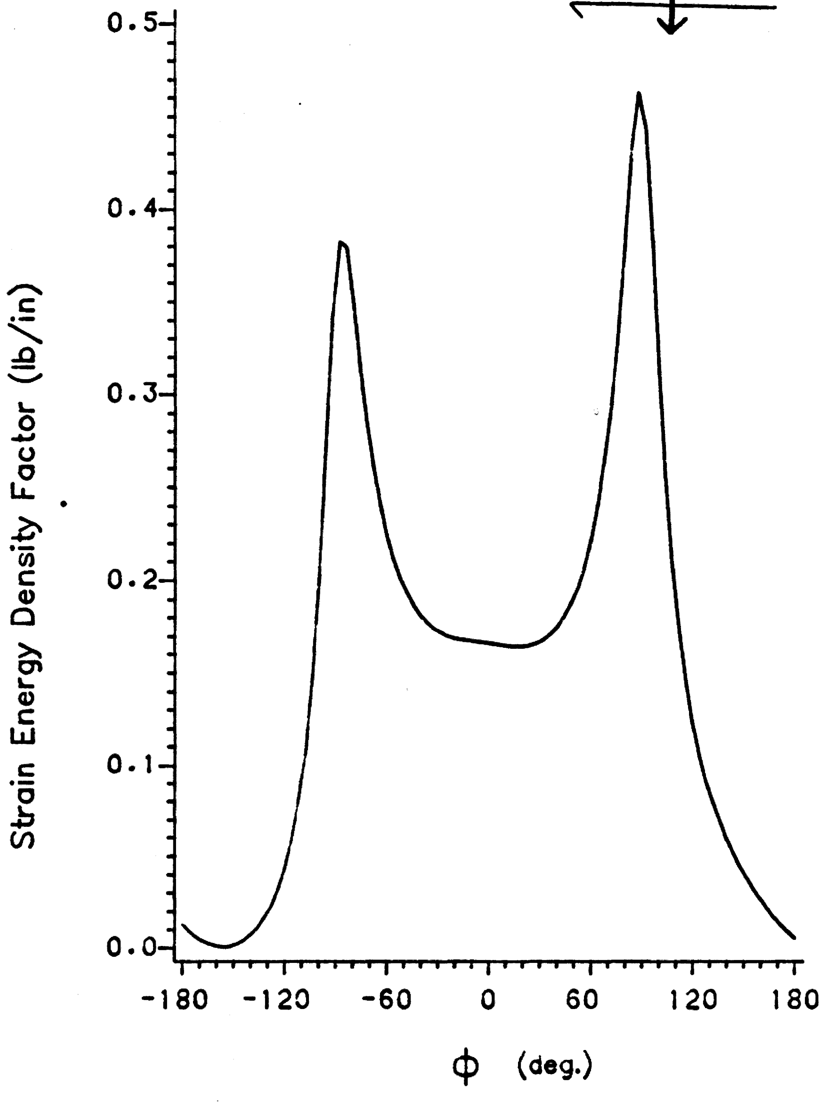

Fig. 4.9 Strain Energy Density Factor Versus Angle ϕ
(specimen with an aspect ratio of 1)

4.2.6 Results with the Normal Stress Ratio

The results obtained for the direction of propagation are summarized in Table 4.2. A typical plot of the normal stress ratio is given in Fig. 4.9 showing a narrow peak whose maximum differs from the experimental result by only 2°. The differences with the experimental values are always equal to or less than 3°.

4.2.7 Results with the Traction Ratio

From the results in Table 4.2, it appears that the predicted angle of propagation varies from 2° to 18° from the experimental results. The predicted loads causing crack initiation are fairly close to the experimental results, but, like the tensor polynomial, show too much sensitivity to the aspect ratio. The influence of the angle α is well represented, almost as well as for the tensor polynomial (A_2 = 0.38).

A plot of the traction ratio factor is given in Fig. 4.11. The maximum is less sharp than in the case of the normal stress ratio.

4.2.8 Conclusion

The superiority of the normal stress ratio for predicting the angle of propagation for these particular cases is obvious. The predictions obtained from the traction ratio are fairly close to the correct results, but not as good. The tensor polynomial often gives rather good results, but is more irregular and sensitive to r_0.

As far as the load at failure is concerned, the three criteria are more difficult to classify, none of the theories represent best

AS4/3501-6

$\alpha = -15.^{0}$ $\theta = 75.^{0}$

$a = 0.1"$ $r_0 = 0.0029"$

Predicted load at failure

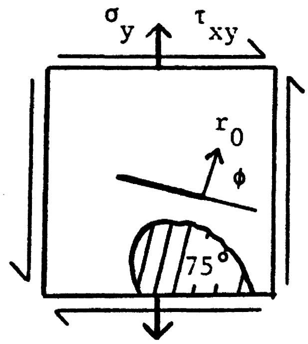

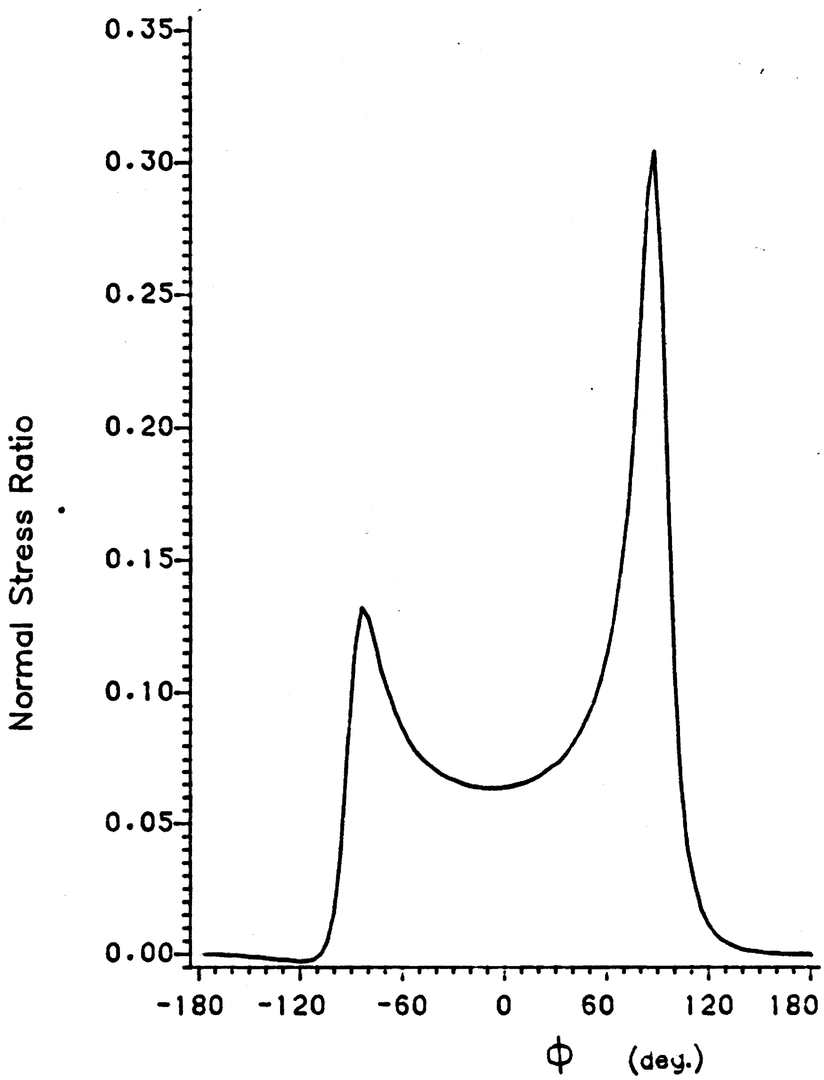

Fig. 4.10 Normal Stress Ratio Versus Angle ϕ (specimen with an aspect ratio of 1)

AS4/3501-6

$\alpha = -15.^0 \quad \theta = 75.^0$

$a = 0.1" \quad r_0 = 0.0029"$

Predicted Load at failure

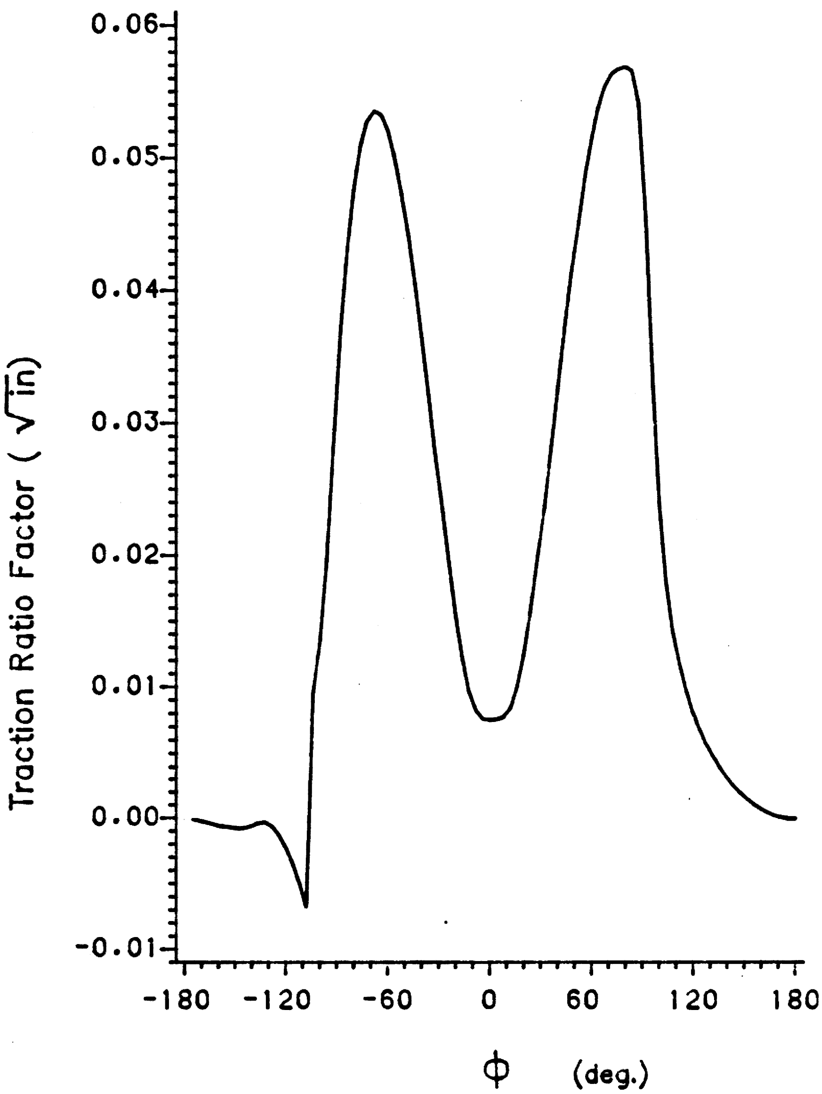

Fig. 4.11 Traction Ratio Factor Versus Angle ϕ (specimen with an aspect ratio of 1)

Table 4.2 Experimental and Predicted Load at Failure and Direction of Crack Extension for AS4-3501 Gr/Ep.

	Tensor Polynomial		Strain Energy Density		Traction Ratio		Normal Stress Ratio	Experimental
	σ_y and ϕ_c	$\Delta\sigma_y$	σ_y and ϕ_c	$\Delta\sigma_y$	σ_y and ϕ_c	$\Delta\sigma_y$	ϕ_c	σ_y and ϕ_c
1A	9139 97°	19%	8559 18°	11%	9084 80°	18%	88°	7710 90°
1H	10032 82°	25%	8770 -24°	8%	9633 57°	20%	72°	8020 75°
4A	6960 100°	3%	7846 -30°	16%	7238 87°	7%	88°	6760 90°
4H	7532 84°	15%	7947 -43°	11%	7876 72°	12%	73°	9810 75°
8A	5775 180°	24%	7330 -41°	3%	6348 88°	16%	88°	7585 90°
8H	6364 85°	30%	7319 -54°	19%	6669 73°	26%	74°	9000 75°
A_1	$1.83\ 10^7$		$0.62\ 10^7$		$1.27\ 10^7$			
A_2	0.034		0.078		0.038			

The specimen are designated by a figure denoting the aspect ratio (1, 4 or 8) and a letter denoting the crack angle (H for a crack perpendicular to the loading and A for a crack prependicular to the fibers).

The loads σ_y are in psi. $\Delta\sigma_y$ is the difference with the experimental result in percentage.

the different tendencies of the epxerimental results. It is interesting to note that the load at failure can be correctly predicted by the tensor polynomial and the strain energy density even through the predicted angle of crack does not correspond to the matrix crack experimentally observed.

A matrix model of the strain energy density would be very interesting to examine, but the computations involved may be overwhelming, and may require a finite element code to obtain the results.

5.0 Conclusions

This study has been concerned with the comparison of four criteria of crack growth in unidirectional composites. The theoretical/experimental correlation is clamined and a new criterion for predicting the critical load and the direction of crack extension has been presented.

For the cases analysed, the normal stress ratio has proven to be consistent crack extension direction criteria. Its main advantages are that it does not involve any other parameter than the elastic and strength constants, and it shows a strong and precise peak in the direction of crack extension.

The tensor polynomial criteria has shown high sensitivity to the strength constants and the chacteristic parameter r_0, which makes its application difficult and sometime impossible. It also exhibited an inability to predict correctly the direction of crack extension in certain fundamental cases. However, in some cases this criteria gives fair results concerning the direction of crack extension, and good predictions as far as the critical load is concerned.

The strain energy density criteria has been shown to exhibit ease of application and little few sensitivity to the parameters involved. It was also shown to predict well the critical load in the cases examined here. However, its failure to give a correct prediction of crack extension direction or even any prediction in certain fundamental cases, and its misrepresentation of a certain trend observed in experimental data points to the need for caution in applying this criteria as well as for further investigations.

The traction ratio theory appears to be a promising criteria for both the prediction of the crack extension direction as well as the prediction of the critical load. Its principal advantage is a relative insensitivity to the parameters involved. However, more theoretical/experimental correlation is needed to critically assess the theory.

References

1. Sih, G. C., "A Special Theory of Crack Propagation," Method of Analysis and Solutions of Crack Problems, Noordhoff Int., XXI, 1972.

2. Sih, G. C., Chen, E. P., Huang, S. L., and McQuillen, E. M., "Material Characterization on the Fracture of Filament-Reinforced Composites," Journal of Composite Materials, Vol. 9, April 1975.

3. Sih, G. C., and Chen, E. P., Mechanics of Fracture, Vol. 16, Martinus Nijhoff Publishers, 1981.

4. Wu, E. M., "Phenomenological Anisotropic Failure Criterion," Composite Materials, Vol. 2, Mechanics of Composite Materials, edited by G. P. Senoleckyz, Academic Press, New York and London, 1974.

5. Wu, E. M., "Failure Criteria to Fracture Mode Analysis of Composite Laminates," Advisory Group for Aerospace Research and Development Conference Proceedings, AGARD-CP-163, North Atlantic Treaty Organization, 1974.

6. Gregory, M. A., and Herakovich, C. T., "Prediction of Crack Extension Direction in Unidirectional Composites," VPI-E-84-27, College of Engineering, Virginia Polytechnic Institute and State University, Blacksburg, Virginia, 1982.

7. Whitney, J. M., and Nuismer, R. J., "Stress Fracture Criteria for Laminated Composites Containing Stress Concentration," Journal of Composite Materials, Vol. 8, July 1984, pp. 253-265.

8. Sih, G. C., and Chen, E. P., "Fracture Analysis of Unidirectional Composites," Journal of Compoiste Materials, Vol. 7, April 1973, pp. 230-244.

9. Poe, C. C., and Sova, J. A., "Fracture Toughness of Boron/Aluminum Laminates with Various Proportionas of 0° and ±45° Plies, NASA Technical Paper 1707, Nov. 1980.

10. Hedgepeth, J. M., and Van Dyke, P., "Local Stress Concentration in Imperfect Filamentary Composite Materials," Journal of Composite Materials, Vol. 1, pp. 294-309.

11. Lekhnitskii, Theory of Elasticity of an Anisotropic Elastic Body, Holden-Day Inc., San Francisco, 1963.

12. Savin, G. N., Stress Concentration Around Holes, Pregamon Press, New York, 1961.

13. Lo, K. H., and Wu, Konishi, D. Y., "Failure Strength of Notched Composite Laminates," Journal of Composite Materials, Vol. 17, September 1983, pp. 383-398.

14. Buczek, M. B., and Herakovich, C. T., "Direction of Crack Growth in Fibrous Composites," Mechanics of Composite Materials, AMD-Vol 58, edited by G. J. Dvorak, American Society of Mechanical Engineers, New York, 1983.

15. Hashin, Z., "Failure Criteria for Unidirectional Fiber Composites," Journal of Applied Mechanics, Vol. 47, June 1980, pp. 329-334.

16. Jones, R. M., Mechanics of Composite Materials, McGraw-Hill Book Company, 1975.

17. Herakovich, C. T., Gregory, M. A., and Beuth, J. L., Jr., "Crack Growth Direction in Unidirectional Off-Axis Graphite-Epoxy," Proceedings of European Mechanics Colloquium 1982, Mechanical Chracterization of Load Bearing Fibre Composite Laminates, A. H. Cardon, editor, Brussels, Aug. 1984.

18. Pagano, N. J., and Halpin, J. C., "Influence of End Constraints in the Testing of Anisotropic Bodies," Journal of Composite Materials, Vol. 2, 1968, pp. 18-31.

19. Hahn, H. T., "A Mixed Mode Fracture Criterion for Composite Material," Composites Technology Review.

20. Sinclair, J. H., and Chamis, C. C., "Fracture Mode in Off-Axis Fiber Composites," Polymer Composite, Vol. 2, Number 1, January, 1981.

21. Tamate, O., Sekin, H., Yosawa, "Discussion on Criteria for Crack Initiation in the Immediate Vicinity of Sharp Edges of Dispersed Inclusion," Journal of Composite Materials, Vol. 16, Sept. 1982, p. 423.

Appendix A

Determination of the Critical Problem Parameters

The determination of the critical load using the strain energy density, the traction ratio and tensor polynomial theories requires the knowledge of the material constants S_c, TF_c and r_o, respectively. In this study, they have been determined in order to obtain the best fit with experimental results. Let us call u_c the parameter (here S_c, TF_c or r_o) to be determined, and $\sigma^p_{yi}(u)$ the predicted axial loading at failure for a specimen i, defined as a function of u.

The best fit with experimental results has been defined here such as, if σ^e_{yi} are the experimental values, the function

$$A_1(u) = \Sigma_i(\sigma^p_{yi}(u) - \sigma^e_{yi})^2 \tag{A.1}$$

is minimum. This can be written mathematically as

$$\frac{\partial}{\partial u}\,[\Sigma_i\,(\sigma^p_{yi}(u) - \sigma^e_{yi})^2] = 0 \quad \text{at } u = u_c$$

or

$$\Sigma_i\,(\sigma^p_{yi}\,(u) - \sigma^e_{yi})\,\frac{\partial\sigma^p_{yi}(u)}{\partial u} = 0 \quad \text{at } u = u_c \tag{A.2}$$

In the case when the predicted loading σ^p_{yi} is a linear function of the parameter u, then for an arbitrary value of u, u_0,

$$\frac{\partial\sigma^{p}_{yi}(u)}{\partial u} = \frac{\sigma^{p}_{yi}(u_0)}{u_0} \tag{A.3}$$

and,

$$\sigma^{p}_{yi}(u) = \sigma^{p}_{yi}(u_0)\,\frac{u}{u_0} \tag{A.4}$$

so that,

$$\frac{\partial A_1}{\partial u} = \sum_i \left(\sigma^{p}_{yi}(u) - \sigma^{e}_{yi}\right)\frac{\partial\sigma^{p}_{yi}(u)}{\partial u} = \sum_i \left(\frac{\sigma^{p}_{yi}}{u_0}\,u - \sigma^{e}_{yi}\right)\frac{\sigma^{p}_{yi}(u_0)}{u_0} \tag{A.5}$$

which gives,

$$u_i = u_0\,\frac{\sum_i \sigma^{e}_{yi}\;\sigma^{p}_{yi}(u_0)}{\sum_i \left(\sigma^{p}_{yi}\;(u_0)\right)^2} \tag{A.6}$$

This is the case of the traction ratio, therefore,

$$TF_c = TF\,\frac{\sum_i \sigma^{e}_{yi}\;\sigma^{p}_{yi}\;(TF)}{\sum_i \left(\sigma^{p}_{yi}(TF)\right)^2} \tag{A.7}$$

In the case of the strain energy density, the loading is a linear function of the square root of S_c, therefore,

$$S_c = S \left[\frac{\sum_i \sigma^e_{yi}\, \sigma^p_{yi}(S)}{\sum_i \left(\sigma^p_{yi}(S)\right)^2} \right]^2 \tag{A.8}$$

the determnation of the radius r_o for the tensor polynomial is more difficult as the tensor polynomial function is nonlinear with respect to the variable r_o, and also because the variables ϕ and r_o are coupled. A simple numerical scheme has been used here. The equation A.2 has been solved by a Newton method:

If a_n is a series defined by an initial value a_1 and:

$$a_{n+1} = a_n - \frac{\sum_i \left(\sigma^p_{yi} - \sigma^e_{yi}\right) \frac{\partial \sigma^p_{yi}}{\partial r}}{\sum_i \left(\sigma^p_{yi} - \sigma^e_{yi}\right) \frac{\partial^2 \sigma^p_{yi}}{\partial r^2} + \left(\frac{\partial \sigma^p_{yi}}{\partial r}\right)^2} \tag{A.9}$$

Then a_n should converge to r_0 optimal if a_1 is not too far from the correct answer. Practically, $\frac{\partial \sigma^p_{yi}}{\partial r}$ and $\frac{\partial^2 \sigma^p_{yi}}{\partial r^2}$ have been evaluated approximately by

$$\frac{\partial\sigma^p_{yi}}{\partial r} = \frac{\sigma^p_{yi}\ (r = \Delta r) - \sigma^p_{yi}(r - \Delta r)}{2\Delta r}$$

$$\frac{\partial^2\sigma^p_{yi}}{\partial r^2} = \frac{\sigma^p_{yi}(r + \Delta r) + \sigma^p_{yi}(r - \Delta r) - 2\sigma^p_{yi}(r)}{(\Delta r)^2} \qquad \text{(A.10)}$$

Δr being a small increment of r.

Appendix B

This section is included to provide additional information concerning the prediction of crack extension by the four criteria previously described. The variation of the tensor polynomial, the normal stress ratio, the strain energy density factor and traction ratio factor are plotted versus ϕ for the Gr/Ep specimens studied in detail in section 4.2. These curves are given for a far-field loading corresponding to the experimental loads at failure.

The specimens are designated by a figure denoting the aspect ratio (1,4 or 8) and a letter denoting the crack angle:

- A for the specimen with a crack perpendicular to the fibers.
- H for the specimen with a crack perpendicular to the loading direction.

AS4/3501-6

$\theta = 75.^0$

$a = 0.1"$ $r_0 = 0.0029"$

Experimental loads at failure

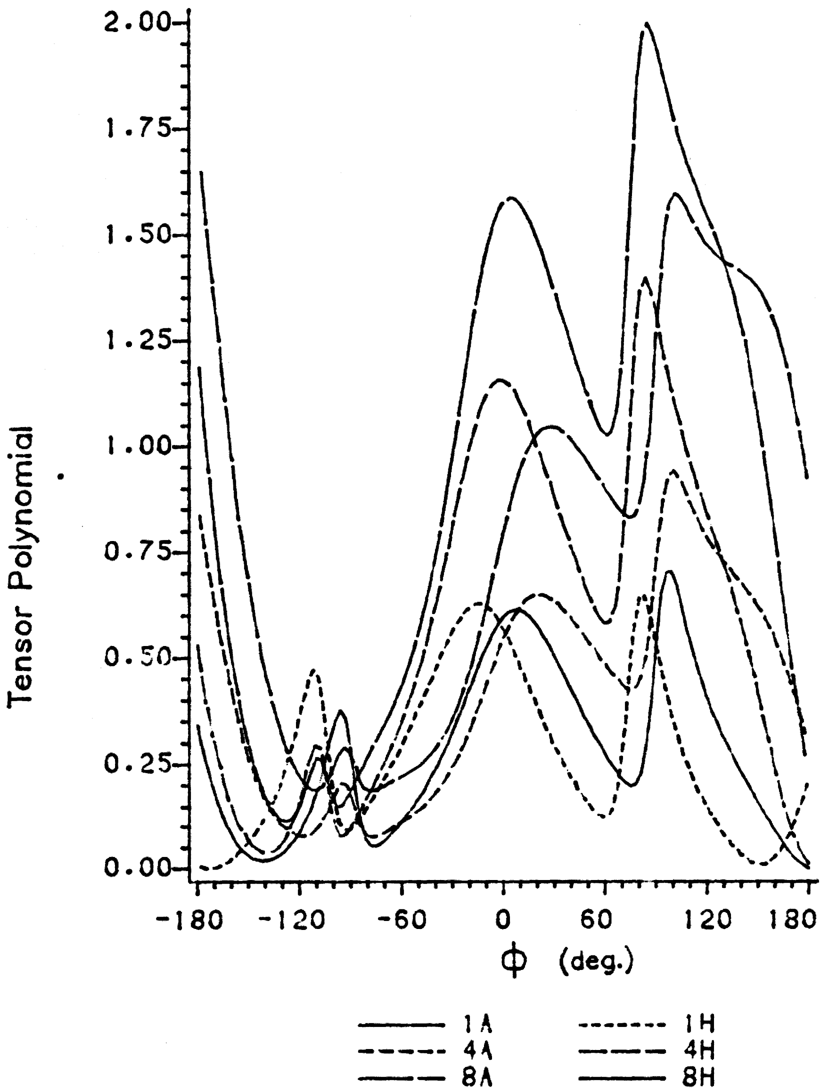

Fig. B.1 Tensor Polynomial Versus Angle θ

AS4/3501-6

$\theta = 75.^{\circ}$

a = 0.1" r_0 = 0.0029"

Experimental loads at failure

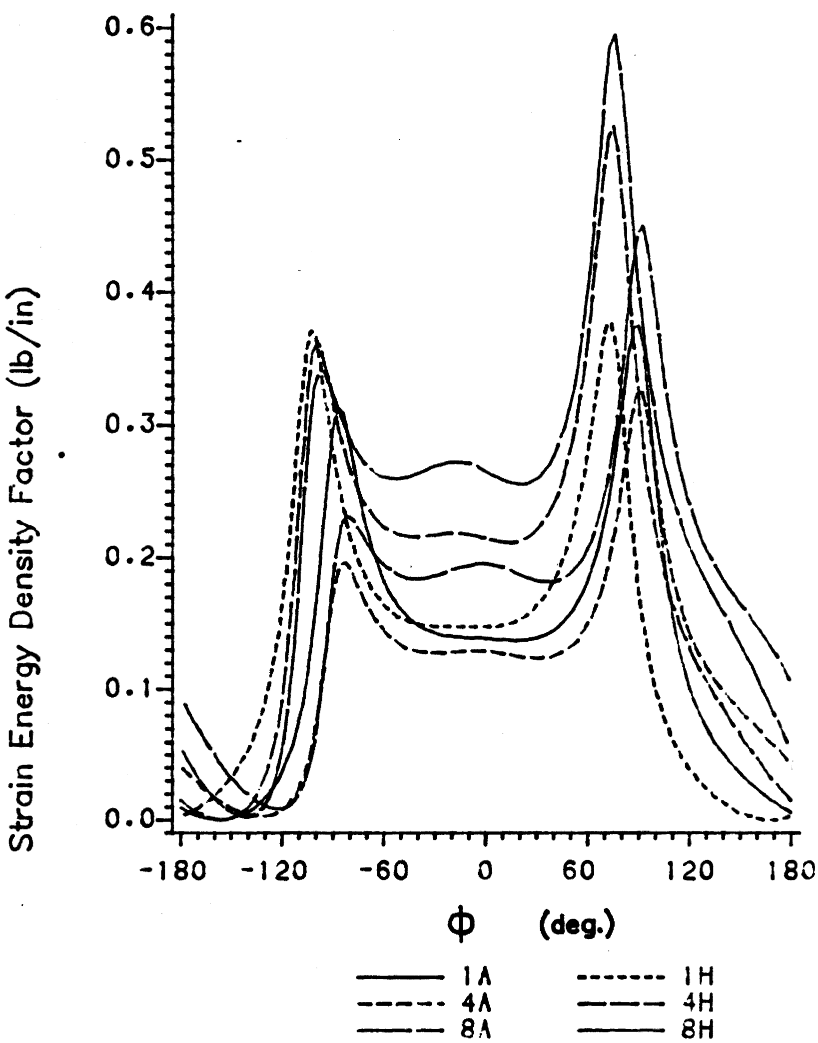

Fig. B.2 Strain Energy Density Factor Versus Angle ϕ

AS4/3051-6

$\theta = 75.^{0}$

$a = 0.1"$ $r_0 = .0.0029"$

Experimental loads at failure

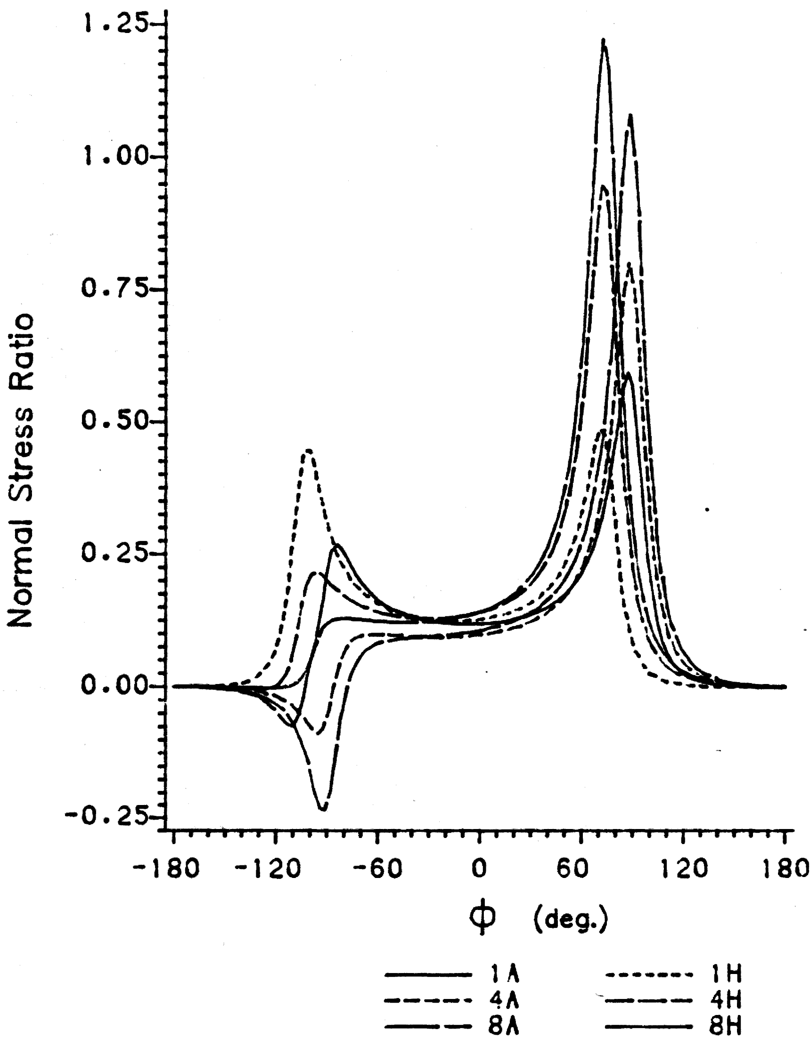

Fig. B.3 Normal Stress Ratio Versus Angle ϕ

AS4/3501-6

$\theta = 75.^{0}$

$a = 0.1"$ $r_0 = 0.0029"$

Experimental loads at failure

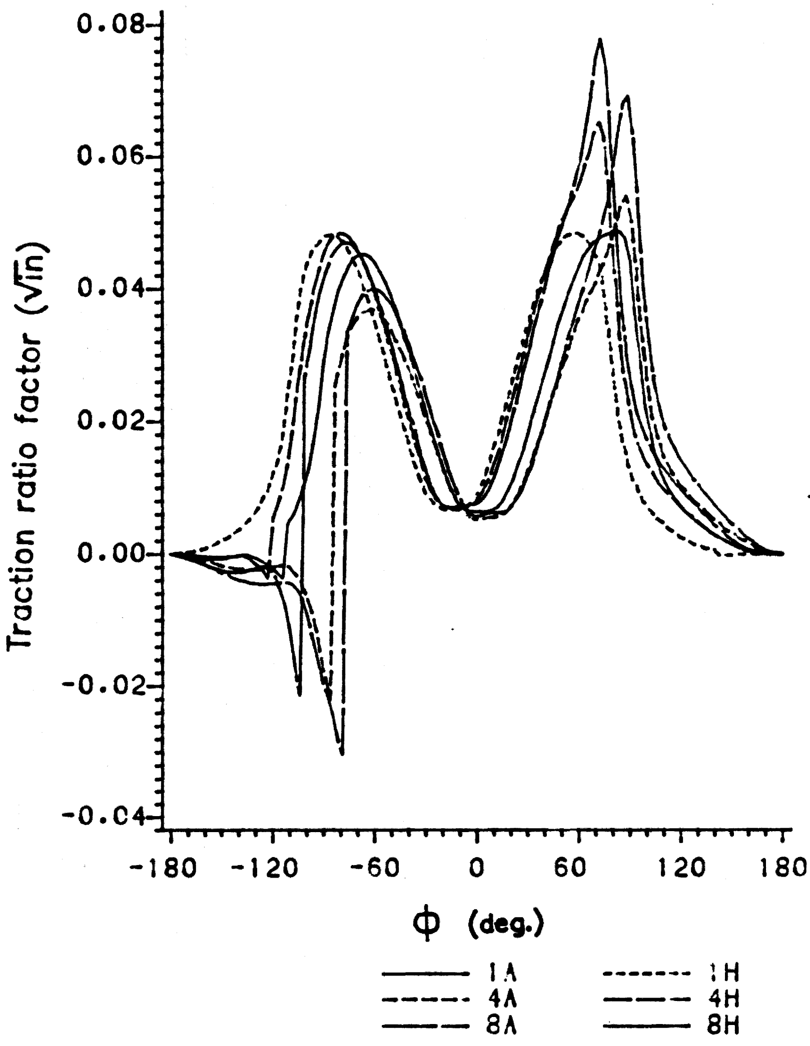

Fig. B.4 Traction Ratio Factor Versus Angle ϕ

Appendix C

Material Properties

BORON ALUMINUM

E_1 = 237 Gpa	X_t = 1672 Mpa
E_2 = 143 Gpa	X_c = -3034 Mpa
G_{12} = 97.8 Gpa	Y_t = 110 Mpa
ν_{12} = 0.23	Y_c = -289 Mpa
	S = 165 Mpa

T300/5208 Graphite/Epoxy

E_1 = 10.2 Msi	X_t = 219.5 ksi
E_2 = 1.56 Msi	X_c = -246 ksi
G_{12} = 0.82 Msi	Y_t = 6.35 ksi
ν_{12} = 0.24	Y_c = -23.8 ksi
	S = 12.5 ksi

AS4/3501-6 Graphite/Epoxy

E_1 = 21.6 Msi	X_t = 282 ksi
E_2 = 1.96 Msi	X_c = -282 ksi
G_{12} = 0.83 Msi	Y_t = 10 ksi
ν_{12} = 0.28	Y_c = -10 ksi
	S = 14.2 ksi

The vita has been removed from the scanned document